Mapping the secondary star in QQ Vulpeculae

Article (Published Version)

Mon. Not. R. Astron. Soc. **310**, 123–145 (1999)

Mapping the secondary star in QQ Vulpeculae

M. S. Catalán,[1] A. D. Schwope[2★] and Robert Connon Smith[3]
[1]*Department of Physics, Keele University, Keele, Staffordshire ST5 5BG*
[2]*Astrophysikalisches Institut Potsdam, An der Sternwarte 16, D-14482 Potsdam, Germany*
[3]*Astronomy Centre, CPES, University of Sussex, Falmer, Brighton BN1 9QJ*

Accepted 1999 June 29. Received 1999 June 3; in original form 1998 December 14

ABSTRACT

We present high- and medium-resolution phase-resolved far-red spectra of the magnetic cataclysmic variable QQ Vul. The spectra show the Na I doublet absorption features near λ 8190 Å from the cool secondary star, and the lines of He II, O I, Mg II, C I, N I, Ca II and Paschen in emission. Using a Doppler imaging technique, we find that the H I, He II, C I and O I lines have a narrow component originating near the L_1 point and a strong component from the stream, while the Mg II and Ca II emission arises solely from the illuminated hemisphere of the red dwarf. We carry out an exhaustive analysis of the emission- and absorption-line velocities and fluxes seen in the QQ Vul spectrum. By simultaneously fitting the radial velocity and flux information we are able to produce surface maps of each line on the secondary star using a technique analogous to the one employed by Davey. The Na I and Mg II maps show an asymmetric distribution akin to that seen in AM Her. Although the observed velocity semi-amplitudes (K_2) of the lines can potentially be corrected for the effects of irradiation, we find that time-dependent changes in the degree of heating on the secondary can lead to large discrepancies in the results, significant enough to give inconsistent values from data taken at different epochs. We discuss the limitations of the surface mapping method as a means of correcting the observed K_2. Our results also suggest that the emission features from the red dwarf are likely to be formed at quite high levels of the stellar chromosphere, in some cases probably even beyond the L_1 point and inside the Roche lobe of the white dwarf, with the different lines possibly forming at different depths. Using the Na I absorption doublet, we find a velocity semi-amplitude for the secondary star of $K_2 = 219 \pm 6\,\mathrm{km\,s^{-1}}$ and a projected rotational velocity of $v_{\rm rot} \sin i = 110 \pm 15\,\mathrm{km\,s^{-1}}$. Thus we estimate the mass ratio to be $q = 0.54 \pm 0.14$. Based on the results of the best-fitting surface maps on all the lines, and the nature of the phase-dependent variations of the continuum and lines, we infer a binary inclination of $i = 65° \pm 7°$, and obtain a complete set of binary parameters for QQ Vul. We classify the secondary star as M4V from the TiO band ratios.

Key words: binaries: close – stars: fundamental parameters – stars: imaging – stars: individual: QQ Vul – stars: late-type – novae, cataclysmic variables.

1 INTRODUCTION

Polars or AM Her stars (in reference to the prototype) are semidetached binaries comprised of a highly magnetic (10–230 MG) white dwarf accretor (the primary) and a cool low-mass Roche-filling donor star (the secondary). They are a subclass of magnetic cataclysmic variables (MCVs), wherein the white dwarf is thought to be locked in synchronous rotation with the binary. Mass transfer takes place via an accretion column which is formed when the gas stream couples with the field of the white dwarf.

QQ Vul was discovered with the *HEAO-1* low-energy detectors in the 0.15–0.5 keV band and catalogued by Nugent (1983). Spectroscopic, photometric and polarimetric observations by Nousek et al. (1984), immediately following its detection, classified this object as an AM Her type cataclysmic variable, with an orbital period of 222.5 min. The study by Nousek et al. and subsequent observations in the optical and X-ray by Mukai et al. (1986), Mukai & Charles (1987) and Obsorne et al. (1986,

★ Visiting Astronomer, German-Spanish Astronomical Center, Calar Alto, operated by the Max-Planck-Institut für Astronomie, Heidelberg, jointly with the Spanish National Commission for Astronomy.

1987) proved QQ Vul to be quite an unusual star, with many inexplicable brightenings and dips in its light curve which were not easy to reconcile with the current model. More recently, X-ray observations by Beardmore et al. (1995) have revealed time-dependent variations in the light curves (both in shape and intensity), which they suggest are caused by the presence of two-pole accretion on to the white dwarf. However, despite the attention that QQ Vul has had in the past, to date its parameters are not accurately known. The true phasing of the binary was not even known until recently (Schwope 1991; Catalán et al. 1995; Schwope et al. 1999, hereafter Paper II).

With the advent of better instruments and the increase in observations of AM Her-type objects, it was becoming obvious that the emission features in these stars have a multicomponent nature. QQ Vul is no exception (Mukai et al. 1986; Paper II). Furthermore, there was increasing spectroscopic evidence that a narrow low-velocity component in the emission lines followed the movement of the red dwarf (McCarthy, Bowyer & Clarke 1986; Mukai et al. 1986; Mukai & Charles 1987). Mukai & Charles found that the Na I absorption doublet near 8190 Å was present in QQ Vul's far-red spectrum. Using these lines they derived a value for the radial velocity semi-amplitude and some preliminary estimates of the system parameters. Knowing that features from the secondary star are clearly visible in QQ Vul, we obtained medium- and high-resolution far-red spectra to carry out a detailed analysis of the donor star. We aimed to determine accurately the binary parameters using the $v_{\rm rot}\sin i$ technique (Drew, Jones & Wood 1993; Welsh, Horne & Gomer 1995), and to study how heating of the secondary star by the accretion shock regions near the white dwarf would affect these measurements. We also aimed to map the intensity distribution of Na I lines on the surface of the secondary, and to ascertain whether the asymmetric distribution found by Southwell et al. (1995) and Davey & Smith (1996) for AM Her is also present in other magnetic CVs.

The analysis of QQ Vul's spectrum turned out to be quite rewarding, complete with its share of puzzling results. As suspected, nearly all the emission features present in the optical and far-red spectrum exhibit a component arising at or near the irradiated hemisphere of the red dwarf. Some lines, such as the Mg II lines at 4481 Å, were found to form solely on the red dwarf (Catalán et al. 1996; Schwope et al. 1998). QQ Vul was hence the first CV to exhibit unequivocally both the emission from the heated face of the secondary and absorption from its cooler hemisphere. This has allowed us to test the current techniques and results on parameter determination. Furthermore, it has made it possible to study the real distribution of the emission not only based on the Na I originating from the unirradiated hemisphere of the secondary but by actually mapping the emission regions on the secondary directly.

2 OBSERVATIONS AND REDUCTION

The observations presented here were taken between 1991 and 1993, and consist of high- and low-resolution spectroscopy taken on the 4.2-m William Herschel Telescope (WHT) at the Roque de los Muchachos Observatory on the island of La Palma, and medium-resolution spectroscopy taken on the 3.5-m telescope at the Centro Astronómico Hispano Alemán in Calar Alto.

A total of 36 medium-resolution far-red and 38 blue spectra were collected simultaneously at Calar Alto between 1991 July 8 and 10, using the Cassegrain double-beam spectrograph TWIN. The red spectra were taken using a GEC CCD chip and a grating that yielded 52 Å mm^{-1} on the chip. Centred at about 8200 Å, this covered the wavelength range $\lambda\lambda$7550–8800 Å with a resolution of about 2 Å. For the blue spectra the RCA2 CCD chip was used. The wavelength coverage of the blue spectra is $\lambda\lambda$4200–5000 Å, and the resolution is approximately 1 Å (D^{-1} = 36 Å mm^{-1}). The exposure times on both the blue and red spectra were typically between 660 and 720 s. Comparison arc line spectra were taken at frequent intervals, and the spectrum of a nearby spectrophotometric standard was taken on each night to correct for instrumental wavelength response.

On the nights of 1993 August 23–25 a total of 59 QQ Vul far-red high-resolution spectra were collected with the ISIS double spectrograph operating at the Cassegrain focus on the WHT. We obtained simultaneous far-red and blue spectra on the EEV3 CCD chip and TEK1 CCD chip, respectively. In the blue arm, and centred at about λ 4600 Å, the 600 line mm^{-1} grating was used, giving a resolution of $\sim$ 1.5 Å and yielding a wavelength range of $\lambda\lambda$4223–5016 Å. For the far-red spectra, the 1200 line mm^{-1} grating was employed. With the EEV3 chip centred at 8100 Å, this resulted in a resolution of 0.73 Å and a wavelength range of $\lambda\lambda$7940–8388 Å. The exposures were 300 s on both the blue and red data. On average, anarc spectrum was taken every 45–60 min to wavelength-calibrate the spectra and to correct for instrumental flexure and stability. Spectra of nearby spectrophotometric standards were taken in order to remove the telluric absorption features and correct for instrumental wavelength response. M-dwarf standard star spectra were also collected to enable the determination of the rotational velocity of the secondary star. Finally, a nearby field star was also located on the slit to correct for slit losses. Wide-slit spectra were taken for QQ Vul, the comparison star and spectrophotometric standard on every night under photometric conditions.

Two additional low-resolution spectra of QQ Vul and some M-dwarf standards were acquired on 1993 August 24 at the WHT, using the 158 line mm^{-1} grating in the red, to enable spectral typing of the secondary. The resulting spectra have a wavelength range of $\lambda\lambda$5815–9149 Å. To wavelength-calibrate the object and M-dwarf star spectra, copper-argon/copper-neon arcs were taken immediately after every object. A spectrum of the spectrophotometric standard BD+25°3941 (Stone 1977) was also taken to remove the atmospheric absorption features and correct for instrumental wavelength response. Unfortunately, our only spectrum of the standard was partially saturated and, because of bad weather conditions, we were unable to take any more. Although it was possible to correct for the instrumental response, its accuracy is reduced. Thus the errors in the spectral typing determination have been increased to reflect the uncertainties introduced by our fluxing problem.

To improve the signal-to-noise ratio (S/N), on-chip binning in the spatial direction was used on readout. A binning factor of 2 was used on all the spectra. To reduce the dead-time between exposures due to readout of the large chips, a narrow window on the chip during all observations was used. Full phase-coverage of QQ Vul was attained in both observing runs.

The reduction procedure followed was the same for both the 1991 and 1993 blue and red data sets. The only difference lies in the packages used. In the case of the WHT data, after bias subtraction and dividing by the flat-field to correct for medium-scale sensitivity variations of the detector, optimal extraction (Horne 1986), as implemented by the FIGARO software package, was used to reduce the 2D images to 1D spectra (see Dhillon

1990; Shortridge 1991 for more detail). The arc spectra were extracted from the same region on the detector as the target star. These were used to obtain the wavelength scale for each object spectrum by interpolating from the wavelength scales of the two nearest arc spectra. Telluric absorption lines were removed by division by a flux standard star. Finally, to correct for the variations of instrumental response with wavelength and large-scale sensitivity variations, a calibration spectrum was created using the FIGARO tables of standards and procedures. The target spectra were then multiplied by this calibration spectrum, creating flux-corrected spectra. The spectra from Calar Alto were extracted and calibrated using the ESO package MIDAS. Spectrophotometry was possible for the WHT high-resolution spectra as a nearby field star was located in the slit. Although simultaneous comparison star spectra were not obtained for the Calar Alto data, photometric accuracy is estimated to be better than 30 per cent. In this paper we shall discuss the far-red spectra, leaving the blue spectra to be discussed in Paper II.

In order to have a more comprehensive set of spectral type standards, we have included those used in Smith et al. (1997). We used the new ephemeris of QQ Vul given in Paper II

$$T_0(HJD) = 244\,8446.471\,05(48) + E \times 0.154\,520\,11(11) \qquad (1)$$

to find the orbital phase at mid-exposure of each spectrum. The numbers in parentheses indicate the errors in the last digits.

3 THE FAR-RED SPECTRUM OF QQ VUL

The co-added red spectrum of QQ Vul is given in Fig. 1. Using all the spectra, a simple average was carried out in both the medium- and high-resolution (Fig. 1 inset) spectra. This option led to a less defined Na I doublet, but was preferred for line identification purposes because it retained all the features originating from other areas of the binary, including features that might have been averaged out if the spectra had been corrected for the orbital motion of the red dwarf.

In addition to the Na I absorption lines at λ8183 and λ8194 Å, the medium-resolution spectra show a wealth of emission features. Marked in Fig. 1 are the emission lines of O I triplet centred at λ7774 Å, He I at λ7816 and λ8361 Å, Mg II at λ7877 and λ7896 Å, the Ca II triplet at λ8498, λ8542 and λ8662 Å, and the Paschen series. We also have a marginal detection of the O I doublet located at λ8446 Å. All these lines show phase-dependent variations that clearly link them to the binary. The high-resolution spectrum plotted in the inset (Fig. 1) shows the presence of emission lines of He II λ8236 Å and C I λ8335 Å, and a number of weaker lines which include Mg II λ8217 Å, N I λ8223 Å, Ca II λ8250 Å, and H I 8323λ Å from the Paschen series. Since Mg II is present in the spectrum of QQ Vul, the He II emission line near λ8236 Å is possibly a blend of the He II and Mg II at λ8238 Å.

As with the majority of MCVs, most of the emission lines in QQ Vul arise from part of the accretion flow and the heated face of the secondary star. The prominent blue lines in QQ Vul show at least three clear components, one of which is known to originate from the illuminated hemisphere of the secondary star (Catalán et al. 1996; Paper II). In the far-red the component from the secondary is even more dominant, and we found that practically all the visible lines to the red of about 7800 Å follow its movement. Fig. 2 shows trailed spectrograms of the wavelength regions $\lambda\lambda$7860–7910, $\lambda\lambda$8150–8380 and $\lambda\lambda$8400–8800 Å covering a complete orbit of QQ Vul, which clearly illustrate this point. The Na I absorption doublet at λ8183 and λ8194 Å (central panel), which in QQ Vul is known to originate from the non-illuminated side of the secondary (Catalán et al. 1996; Schwope et al. 1998), is included in the figure for comparison. So far, QQ Vul and AM Her are the only MCVs whose Na I surface distribution is confirmed to be significantly affected by heating.

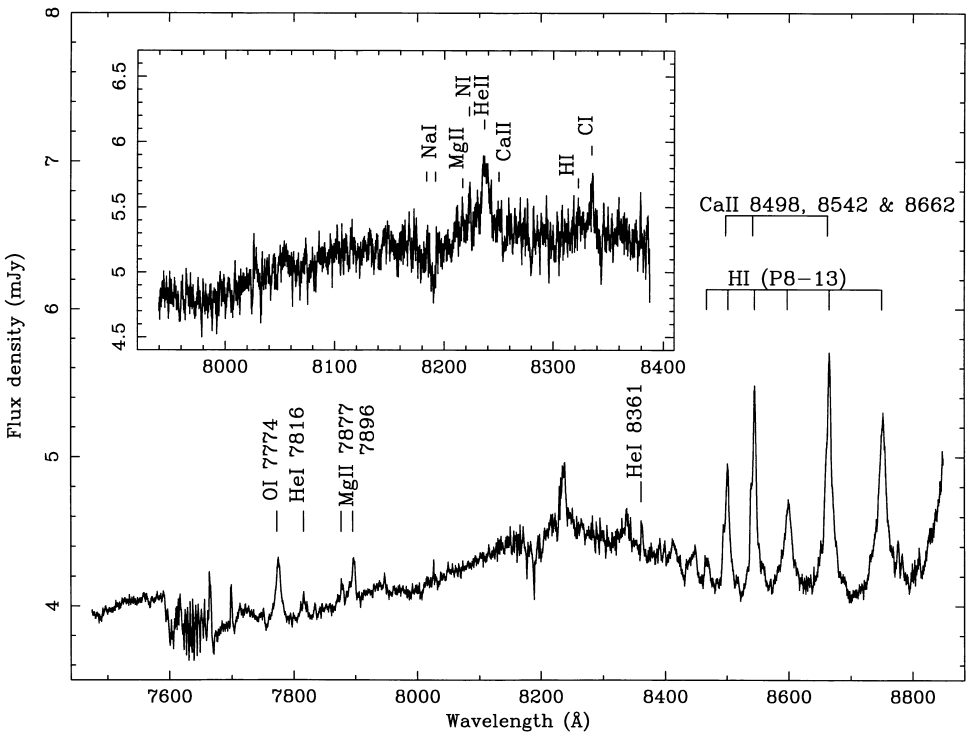

Figure 1. Average medium- and high-resolution (inset) spectrum of QQ Vul uncorrected for the orbital motion of the red dwarf. The identified lines have been marked.

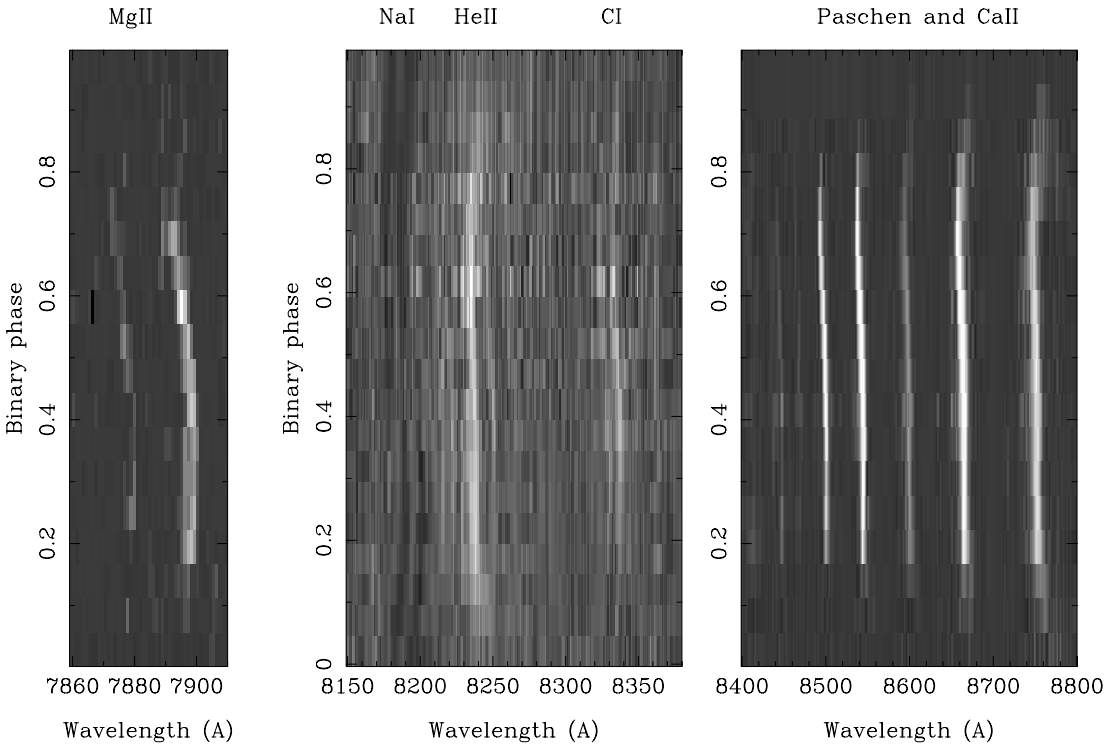

Figure 2. Trailed spectrograms of the regions at either side of the Na I absorption lines covering a full binary orbit. The central panel shows the trails of He II and C I near the Na I lines. The left panel shows the Mg II emission lines at λ7877 and λ7896 Å, and the right panel shows all the Paschen lines. The visible emission lines clearly follow the movement of the secondary.

4 CLASSIFICATION OF THE SECONDARY STAR

The secondary star in QQ Vul was classified using the same quantitative technique as in Wade & Horne (1988). The method requires low-resolution spectra of the object and a number of M-dwarf spectral type standards in the red region of the spectrum, and uses the TiO band flux ratios to obtain the low-mass star spectral type. Since the spectral range and the dispersion of the low-resolution spectra presented here is the same as in Wade & Horne (1988), in order to obtain a better distribution of spectral type standard star TiO measurements, we have opted to use some of their results. A straight line was fitted to the continua of our two object spectra and the spectral type standards in the wavelength regions $\lambda\lambda$7449–7551, $\lambda\lambda$8129–8171 and $\lambda\lambda$8231–8270 Å. Using the continuum fits, the flux density deficits of the TiO bands were determined exactly as in Wade & Horne (1988). We refer the reader to their paper for details of the method.

In Fig. 3 we plot the fractional strength of the TiO flux density $d_\nu(\lambda 7665)$ relative to the continuum flux at λ7500 Å against the TiO $d_\nu(\lambda 7165)/d_\nu(\lambda 7665)$ ratio. The open circles correspond to the derived flux ratios from the data set presented in this work and from the M dwarfs in Smith et al. (1997), and the filled circles are those taken from Wade & Horne (1988). The resulting flux ratios from the average of the two low-resolution QQ Vul spectra are shown with the corresponding error bars. The errors in the measurements have been extended to account for the possible uncertainties in the flux calibration. Our results show that the secondary star in QQ Vul is an M4V star to better than a spectral type. Fig. 3 also indicates that the red dwarf contributes about 15 per cent of the light at λ7500 Å at phase $\phi = 0.1$ when the spectra were taken.

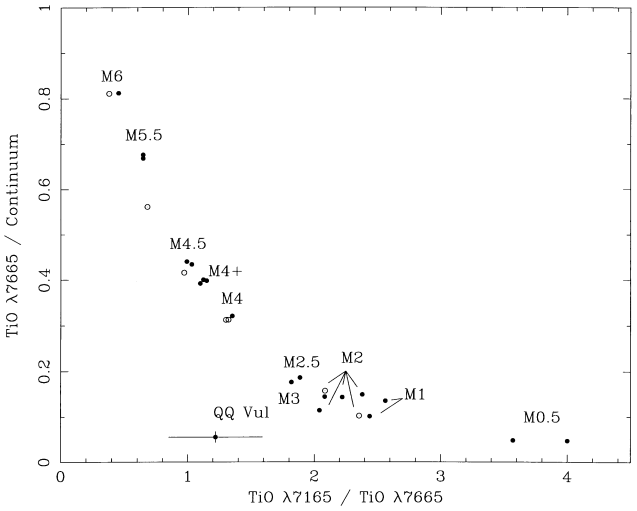

Figure 3. TiO λ7165/continuum shown against the TiO ratio λ7165/λ7665. The spectral type standards from our data set are shown as open circles, and those from Wade & Horne (1988) as filled ones. The average of the TiO ratios of the two QQ Vul spectra is shown with error bars. The spectra were taken at $\phi = 0.1$; thus contamination from the heated face of the secondary to the total light is negligible. It is clear that the spectral type of the secondary star in QQ Vul is later than M3V and earlier than M5V.

5 LINE RADIAL VELOCITIES

The method used to derive the velocity variations of each line with orbital phase depended on whether the line is an absorption or an emission feature. Thus we outline the methods separately.

All the radial velocity variations were fitted with a circular orbit

Table 1. Results of the radial velocity line fits for all the data sets. The column headed 'Type' indicates whether the line was in emission (E) or absorption (A). The year corresponds to the year of the observation. The data from Calar Alto were taken in 1991, and the data from the William Herschel Telescope at La Palma were collected in 1993. The root-mean-square (rms) deviation in column 6 refers to the scatter of the points in relation to the fit.

Line	Type	K_{obs}(circ) ($km\,s^{-1}$)	γ ($km\,s^{-1}$)	ϕ_0 (phase)	rms ($km\,s^{-1}$)	Year
Mg II 4481 Å	E	150 ± 2	−39.8 ± 2.6	0.046 ± 0.003	41	1991
	E	119 ± 2	−15.0 ± 2.1	0.036 ± 0.003	23	1993
Mg II 7877 Å	E	131 ± 5	−21.0 ± 5.6	0.034 ± 0.008	17	1991
Mg II 7896 Å	E	132 ± 3	−37.8 ± 3.0	0.038 ± 0.004	27	1991
Na I 8190 Å	A	271 ± 3	5.3 ± 2.1	0.009 ± 0.002	33	1991
	A	228 ± 2	−0.4 ± 1.5	0.024 ± 0.001	44	1993
He II 8236 Å	E	84 ± 3	5.7 ± 2.1	−0.011 ± 0.006	26	1991
	E	54 ± 3	6.7 ± 2.3	−0.039 ± 0.010	24	1993
C I 8335 Å	E	118 ± 11	12.1 ± 13.4	−0.029 ± 0.019	33	1991
	E	70 ± 4	−1.5 ± 2.6	−0.028 ± 0.008	32	1993
Ca II 8498 Å/	E	143 ± 1	−0.3 ± 1.3	0.009 ± 0.002	26	1991
H I 8502 Å (blend)	E					
Ca II 8542 Å/	E	140 ± 1	−7.2 ± 0.8	0.015 ± 0.001	22	1991
H I 8545 Å (blend)	E					
H I 8598 Å	E	104 ± 4	−24.2 ± 3.5	−0.029 ± 0.007	32	1991
Ca II 8662 Å/	E	141 ± 1	−5.4 ± 1.1	0.014 ± 0.002	16	1991
H I 8665 Å (blend)	E					
H I 8750 Å	E	110 ± 3	−18.8 ± 2.5	0.007 ± 0.004	22	1991

curve of the form

$$V_{circ}(\phi) = \gamma + K \sin 2\pi(\phi - \phi_0), \quad (2)$$

where ϕ is the orbital phase of the observation, γ is the systemic velocity, K is the semi-amplitude of the observed radial velocity curve, and ϕ_0 is the 'cross-over' phase.

Where the same line was present on both the 1991 and 1993 data sets, separate radial velocity measurements were carried out. The results of the fits are given in Table 1. For the four lines common to both data sets we found that there is a difference in the radial velocity semi-amplitude that ranges between 30 and $50\,km\,s^{-1}$, the velocities being consistently higher in the 1991 spectra. It is likely that the differences are the direct consequence of a change in the degree of heating on the secondary in the two epochs. A larger extent of the irradiated region would result in an increased velocity semi-amplitude of the lines as they get pushed further towards the back of the star. The Doppler maps in the next section do suggest that this scenario is quite likely.

5.1 The emission lines

Although some lines such as He II at 8236 Å or the Paschen series showed a component associated with the stream, the most prominent component in the emission lines was generally the one originating from the illuminated face of the secondary star, as shown in Fig. 2. Thus a single-Gaussian model with the appropriate full width at half maximum was usually good enough for obtaining the radial velocities in the binary phase range $\phi = 0.15 - 0.85$ in the stronger lines. The exception was at the binary phases where the stream and secondary star emission components crossed over, i.e., at phases $\phi = 0.1 - 0.25$ and $0.6 - 0.7$. At these phases a multi-Gaussian fit to the line was employed. For some of the weaker emission lines the spectra were binned in phase in order to improve the S/N of the line.

The Mg II emission line doublet at λ4481 Å has also been included in our analysis, because it has previously been found by Catalán et al. (1995) to originate from the red dwarf. This doublet lies very close to the He I emission at λ4471 Å, and is contaminated by it at phases $\phi = 0.0 - 0.2$ and $0.6 - 1.0$. Hence all the points within these phase ranges have not been used in the radial velocity fits.

We have also attempted to obtain the radial velocities of a number of other lines present in this wavelength region, such as O I at 7774 Å and He I at 7816 and 8361 Å, but our results were inconclusive and thus have not been included in Table 1. In the case of the O I line, the secondary star is the primary source of the line only between phases $\phi = 0.45$ and 0.65, which is not enough phase coverage for a reliable fit. The stream component was by far the more dominant one at most phases, unlike the other lines. Nevertheless, we have included its Doppler map in Section 6. For the two faint He I lines we measured very small velocities. They yield a maximum radial velocity semi-amplitude of $30\,km\,s^{-1}$, and appear to follow the movement of the secondary. We also detect phase-dependent variations in the line flux consistent with an origin near the L_1 point. However, the resolution of our spectra is not high enough to give reliable results.

5.2 Na I absorption lines

The radial velocities of the secondary star using the Na I doublet near 8190 Å were obtained by cross-correlation with a template. As with the emission, the two data sets were analysed separately, for various reasons. First, no M-dwarf spectra were observed during the 1991 run, and we did not have M-dwarf spectra in our library that could match the resolution of the 1991 data. Most importantly, however, the two data sets were found to yield significantly different values of the radial velocity semi-amplitude.

In the case of the 1993 high-resolution spectra, where M-dwarf spectral type standard spectra were taken with the same instrumental set-up as the data, the template chosen is the spectrum of an M-dwarf of the nearest spectral type to the secondary in QQ Vul. This corresponds to the Gliese star GL105B, which is classified as an M4.5V star (Gliese 1969) and has a radial velocity of $24.7\,km\,s^{-1}$ (Stauffer & Hartmann 1986). We initially considered binning all the data from all three

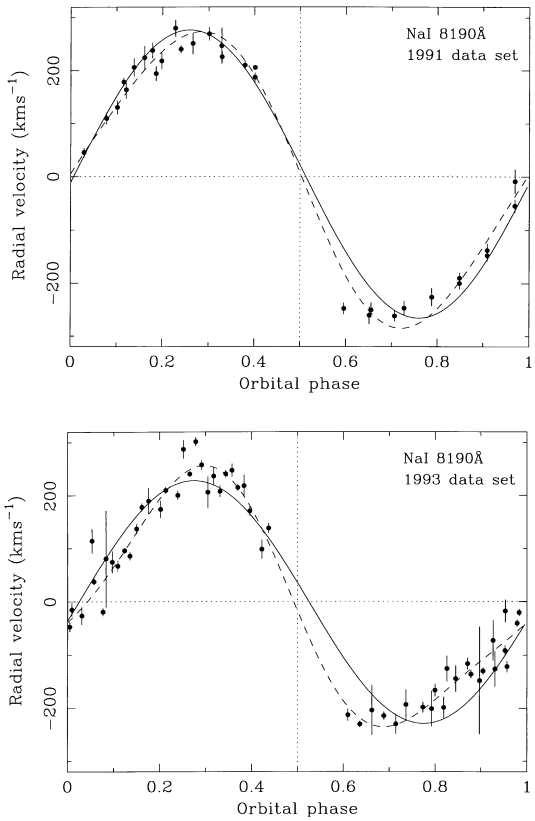

Figure 4. Radial velocity fits to the Na I doublet near 8190 Å for the two data sets. The solid curve corresponds to the circular fit, and the dashed curve is the elliptical fit to the data.

nights in phase to increase the S/N of the lines. However, since we did not have a large enough number of spectra, we found that this had the ill effect of degrading the spectra which clearly showed the Na I lines. In the end we found it better to cross-correlate each spectrum individually and reject those points which gave velocities higher than $\pm 700\,\mathrm{km\,s^{-1}}$. A Gaussian was fitted to the cross-correlation function of each spectrum, and the error in the position of the peak corresponds to the error in the derived velocity. Approximately between phase $\phi = 0.4$ and 0.6 the Na I doublet is practically depleted, explaining the absence of points in this phase region. Because no M-dwarf spectra with a similar resolution were available to use with the 1991 data, the template was constructed using two inverted Gaussians with a constant separation and appropriately scaled so as to mimic the Na I lines. The results were quite satisfactory. As with the 1993 spectra, the Na I lines were not detectable between $\phi = 0.4$ and 0.6. The parameters resulting from the circular fit given by equation (2) are summarized in Table 1. The errors quoted for K, γ and ϕ_0 are the formal errors. A more reliable indication of the goodness of the fit is the root-mean-square deviation of all the points to the fit, which we also list. The best circular fits for both data sets are shown in Fig. 4 as a solid line. It is interesting to note that the radial velocities during maximum blueshift of the secondary found by Mukai & Charles (1987) deviate from the circular fit in almost exactly the same way as the data presented in this paper.

It has long been known that a change in the light distribution on the secondary leads to a deformation of the spectral lines. Therefore the radial velocities determined from them will appear slightly shifted, as the centre of light may not coincide with the centre of mass of the star at a given phase (Martin, Jones & Smith 1987; Wade & Horne 1988; Friend et al. 1990a,b). This results in a fictitious ellipticity in the absorption-line velocities, and it is possible to correct for this if the extent of the illuminated surface of the secondary is known (Davey & Smith 1992). Thus, in addition to the circular fits, we carried out elliptical fits to the observed radial velocity curve with an equation of the form

$$V_{\mathrm{ell}}(\phi) \equiv \gamma + S_1 \sin(2\pi\phi) + C_1 \cos(2\pi\phi) + S_2 \sin(4\pi\phi) + C_2 \cos(4\pi\phi). \quad (3)$$

where S_1, S_2, C_1 and C_2 are fitting parameters. To derive the eccentricity and semi-amplitude of the curve, we used the more general technique described in Smart (1977) as the method of Lehmann–Filhés. The method involves the derivation of the maximum and minimum velocities and the area subtended by the fit of the radial velocity curve. We summarize the results for the elliptical fits in Table 2. We found that the elliptical fits to both data sets, shown as a dashed line in Fig. 4, are statistically better (99 per cent significance) than the circular fits, but the eccentricities that result are quite large particularly in the 1993 data. In their study, Friend et al. (1990a) and Davey & Smith (1992) found the eccentricities to be lower than 0.1 for most of the binaries. We do not know why QQ Vul shows a larger eccentricity, and more during the 1993 than the 1991 observations. Since this is of major relevance to the correction of the observed K_2, we discuss this point in Section 10.

Table 2. Results of the elliptical fits to the Na I absorption lines.

Year	K_{obs}(ell) ($\mathrm{km\,s^{-1}}$)	γ ($\mathrm{km\,s^{-1}}$)	e	rms ($\mathrm{km\,s^{-1}}$)
1991	279 ± 3	-0.2 ± 2.2	0.097 ± 0.007	23
1993	246 ± 2	-8.3 ± 1.6	0.161 ± 0.008	30

6 DOPPLER MAPS

In order to find out exactly where each line originates in the system and to what extent the secondary is illuminated, we carried out a Doppler map analysis on all the lines present in each data set. The technique we used is as employed in Marsh (1988). Further details on the concept, application and interpretation of Doppler maps can be found in Marsh (1988) and Kaitchuck et al. (1994). Unlike the usual disc maps, in our case the lines primarily map at the expected position of the secondary star and, in some cases, the stream.

Since the velocity of the secondary is known to be less than $500\,\mathrm{km\,s^{-1}}$, the maps were constructed using a $1000\,\mathrm{km\,s^{-1}}$ square grid centred at the rest velocity of the system, with pixel sizes appropriate to each data set: 20 and $10\,\mathrm{km\,s^{-1}}$ per pixel for the 1991 and 1993 spectra, respectively. The positions of the centres of mass of the white dwarf, the system and the red dwarf are indicated with crosses. In addition, we have outlined the shape of the red dwarf. The locations of the centres of mass and the red dwarf shape are based on the final parameters we derived (Table 4). The resulting maps are shown in Figs 5 and 6.

In Fig. 5 we have superimposed a grey-scale map of the Na I absorption with a contour plot of an emission line. The 1991 and 1993 data sets are shown on the left- and right-hand panels, respectively. The grey-scale used for the absorption is the same for the two data sets. The contours on the top row show the Mg II 4481-Å, the middle row represents the He II 8236-Å, and the

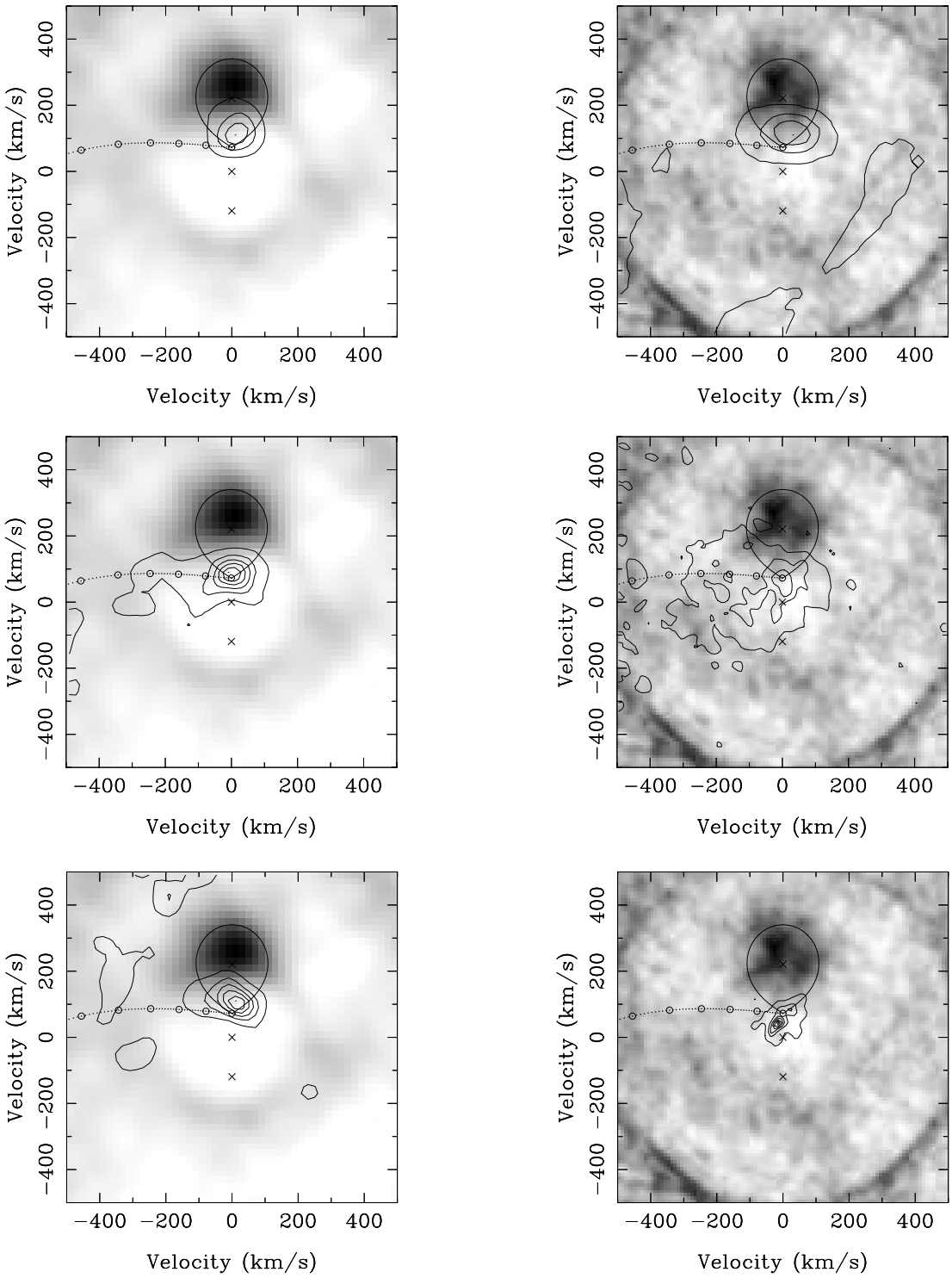

Figure 5. Doppler maps of the prominent lines in the far-red spectrum of QQ Vul common to both 1991 (left column) and 1993 (right column) data sets. The grey-scale corresponds to the Doppler map of the Na I doublet. These are superimposed with the Doppler maps of Mg II 4481 Å (top), He II 8236 Å (middle) and C I 8335 Å (bottom) which are shown as contours. The positions of the centres of mass of the red dwarf, the binary and the white dwarf are indicated with crosses.

bottom row is the C I 8335-Å emission lines. Because the intensities in the resulting Doppler maps between the 1991 and the 1993 data and between the lines differ, the isocontours do not correspond to the same levels in each panel. What are shown are the intensity isocontours above 30 per cent of the total range. The ring around the Na I Doppler map on the 1993 data is an alias caused by a bad pixel. This data set was taken on a higher resolution setting than the 1991 spectra and had much shorter exposures, and is, as a result, noisier. Nevertheless, the maps clearly show that the emission lines do originate near the L_1 point and the heated areas of the secondary star, and that the shape, intensity and extent of the emission varies a lot between the two

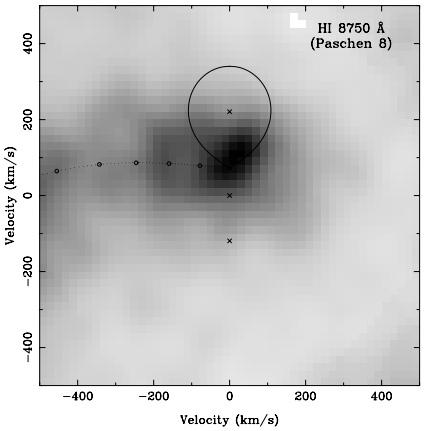

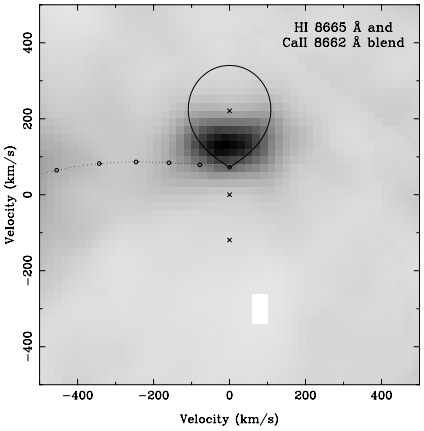

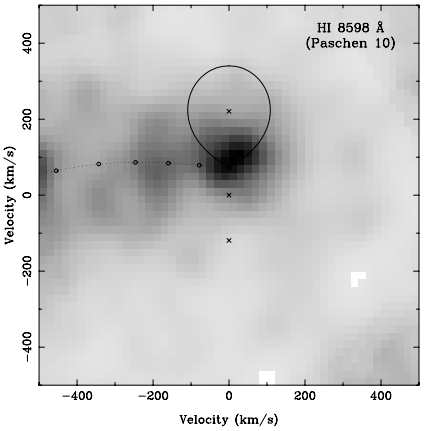

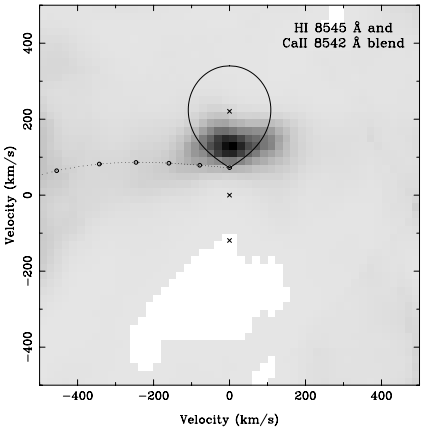

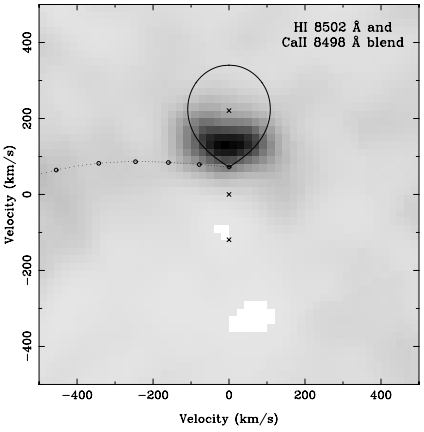

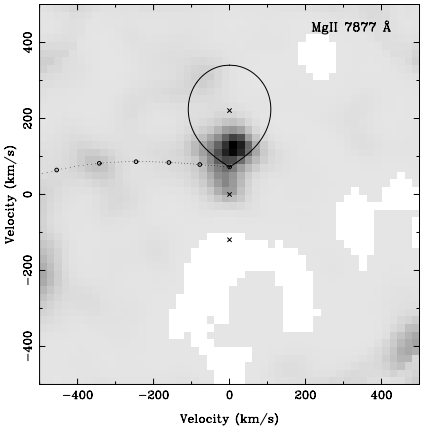

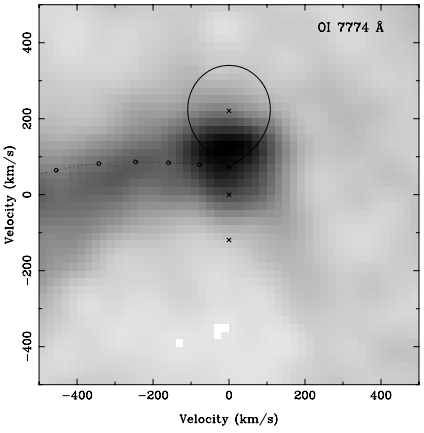

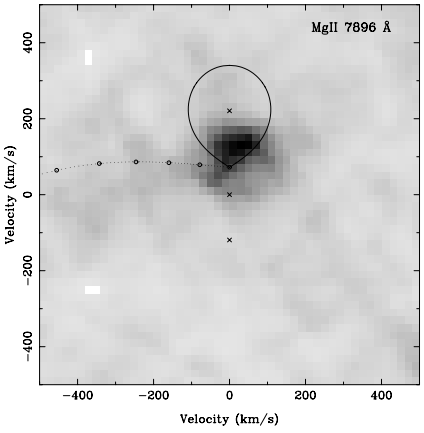

epochs. In particular, the maps of the He II and C I emission and the Na I lines suggest that the secondary was slightly more irradiated during the 1991 observations than in 1993.

Fig. 6 shows the Doppler maps of the other lines detected during the 1991 run. It is immediately obvious that some lines have a distinct stream component, and that in others it is very faint or not there at all. The H I, He II and O I line Doppler maps all show the stream. In addition, we observe an interesting feature in the velocity map located on the opposite side of the stream, relative to the line of centres, centred at approximately $V_x = 100\,\mathrm{km\,s^{-1}}$ and $V_y = -50\,\mathrm{km\,s^{-1}}$. This feature is particularly prominent in the O I and Paschen 8 emission line on the Doppler maps shown in Fig. 6, but not in the Paschen lines which are blended with Ca II. We believe that the Ca II component from the secondary towers above the H I, making the stream component appear relatively weak. Unfortunately, it is not possible to know the exact location of this material in position coordinates. It appears to lie parallel to the path of one Keplerian orbit of the stream. One could speculate on the possibility that some stream material might be slung by the field (rather than captured) allowing it to go further before being recaptured, but the likelihood of it being able to go round seems remote. We consider it more probable that these velocities correspond to the material in the region where the stream interacts with the magnetic field of the white dwarf or thereabouts.

There are other interesting features in the maps which are worth mentioning. One is that the stream has a 'blobby' appearance in the Paschen lines that are not blended with Ca II and the He II line in the 1991 spectra. It may well be that this apparent structure is not real. An overfit using MEMSYS can intensify the noise in the data if pushed too far, thus creating false features. However, in our case, the more obvious structures in the Doppler maps are similar in these three lines. The second observation is the asymmetry of the mapped Mg II emission lines. Although some of the other emission is also asymmetric (e.g., the H I 8598-Å line in Fig. 6), the largest asymmetries relative to the line of centres are found in the Mg II maps (Figs 5 and 6). It is quite extreme in the case of the Mg II 7896-Å line. Finally, there is a spread in the emission-line velocities that extends in the region of the L_1 point and near the centre of mass of the system in a number of emission lines.

7 LINE FLUX PHASE-DEPENDENT VARIATIONS

Line flux variations originating from the secondary star can also be a useful tool for studying the intensity distribution of the line on the stellar surface. The technique applies to both the emission and the absorption lines. It was used successfully in a detached system by Catalán et al. (1994), who mapped the Hα emission line on the secondary. Similarly, Davey (1994) obtained encouraging results when he tested it in a number of CVs. The main disadvantage in CVs is that the variations of the line flux with phase may not be totally attributable to the secondary star irrespective of whether the line originates from it. None the less, used in conjunction with the radial velocities, this provides some extra information in the line.

One of the reasons why equivalent widths are not typically used in CVs is the large variability of the continuum flux. Since the line and the continuum sources could be different, we have opted to use the total flux of the line above the continuum, for the emission lines, and below the continuum, in the case of the absorption lines, for our analysis. To get accurate fluxes one would require a comparison star on the slit during the observations. This corrects for small-scale variations in flux due to slit losses and changes in the observing conditions. A comparison star was located in the slit during the 1993 run but not in the earlier set of observations. However, the observing conditions during the 1991 run were found to be very stable as the line variations matched the later data quite well. The relative changes in the line within the same run were consistent between the different nights of the run as well.

The total line fluxes were estimated as follows. A low-order polynomial fit to the continuum was first subtracted from the spectra. Then the total area in the line was estimated either by summing up all the flux within the line region, if the primary component of the line comes from the secondary star, or by using a three-Gaussian fit, if various components are present in the line. In the latter case, only the flux of the Gaussian corresponding to the secondary component was used to create the surface maps. Reliable line flux measurements of the emission lines with prominent stream components were possible only between phases $\phi = 0.2$ and 0.8. The combined flux deficits of the Na I absorption lines were also derived in a similar fashion, except here the spectrum was subtracted from the continuum fit to keep the numbers positive. Due to the lower S/N of the Na I lines in the 1993 data, it was necessary to bin the spectra in phase to get reasonable measurements. As the surface mapping program requires the same number of radial velocity and line flux points when fitting both sets of information simultaneously,we used the average flux for a given phase bin region to be the flux of all the spectra included in that phase bin. The line fluxes are shown together with the radial velocities and the resulting surface map fits for Na I in the next section.

The emission component from the secondary star was so prominent in the blended Ca II and Paschen lines in QQ Vul that the phase-dependent line flux variations clearly show the characteristic behaviour seen in the irradiated M dwarfs of detached white dwarf-red dwarf or pre-CV binaries. In Fig. 7 we show the line light curves of the Ca II 8542 Å and Paschen 11 blend as an example. The other emission features from the secondary also exhibit the same behaviour, though not as marked as in the previous case. They are generally much weaker than the Ca II line, and are more likely to be affected by emission from the stream. However, the general trend is the same. The flux of the line reaches maximum at around phase $\phi = 0.45$. We have also plotted in Fig. 7 the flux variation in phase of the Mg II 7877-Å and He II 8236-Å lines. The noticeable hump in the light curves between phases $\phi = 0.1$ and 0.3 is likely to be caused by a faint stream component in the line, which is relatively stronger in the He II line than in the others. At these phases the emission component from the stream overlaps with the one originating from the secondary making them hard to disentangle with the three-Gaussian fit. Note that even the Ca II/Paschen blend shows this kink.

Figure 6. Doppler maps of the emission lines in the 1991 medium-resolution data set.

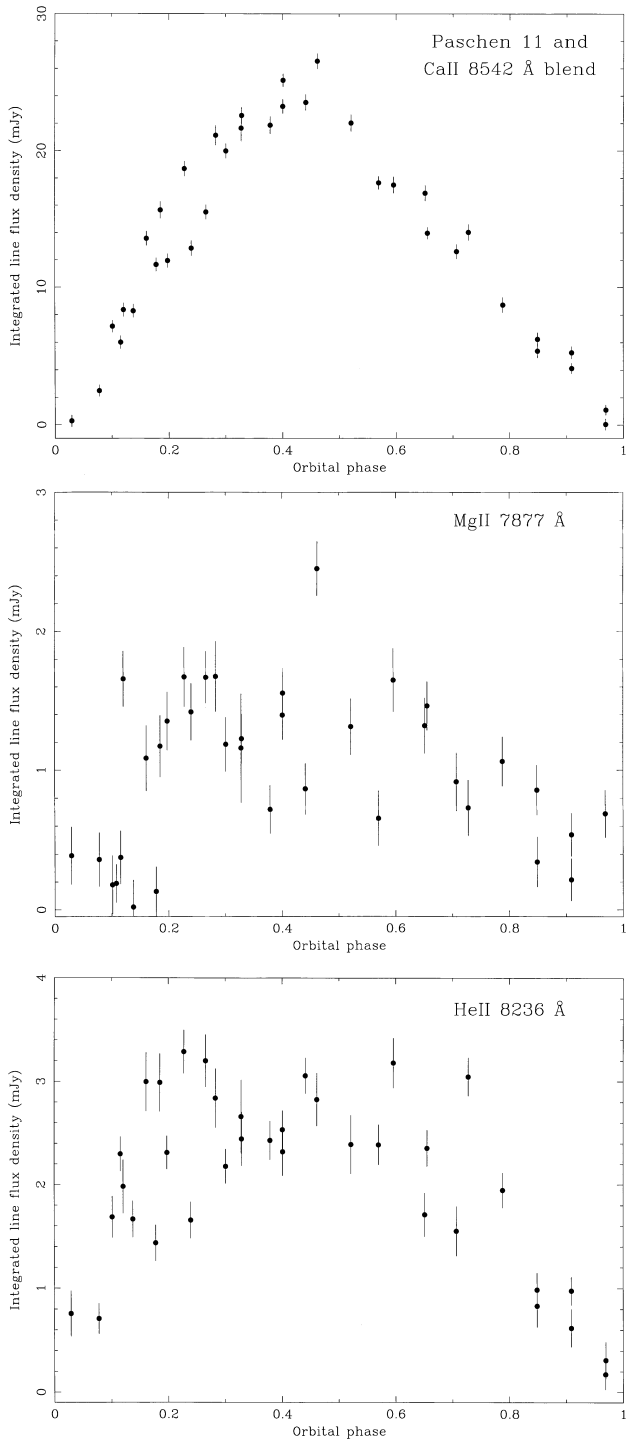

Figure 7. Integrated flux densities of the Ca II 8542 Å and H I 8545 Å blend, Mg II 7877 Å and He II 8236 Å in the 1991 data set against orbital phase.

8 SURFACE MAPS OF THE SECONDARY STAR

Heating on one side of the secondary star leads to the deformation of the spectral lines originating from it. Therefore the radial velocities determined from them will appear slightly shifted, as the centre of light may not coincide with the centre of mass of the star at a given phase. In CVs, the effect was first reported by Joy (1954) in his study of AE Aqr. Joy found that the radial velocity curve showed an ellipticity which was not due to a simple elliptical motion of the secondary, and was more likely caused by variations in the centre of light of the lines. More recent studies, this time of IP Peg (Martin et al. 1987), of Z Cam (Wade & Horne 1988) and in the extensive survey by Friend et al. (1990a,b), found similar ellipticities in the absorption-line velocities and clear signs of time-dependent changes in the shape of the lines.

If the extent of the reprocessing surface on the secondary star is known, it is possible to correct the radial velocity curve to account for it. Friend et al. (1990a,b) found that an elliptical fit to the radial velocity curve was appropriate for modelling the distortion. They proposed that by measuring the departure of the fit from a circular one, it is possible to correct for the radial velocity semi-amplitude obtained. Davey & Smith (1992) took the idea one step further. By assuming that the velocity distortions are wholly due to the uneven heating of the secondary, and that contamination from the disc or any other areas of the binary is unimportant, the departure of the radial velocity curve from a circular one (what Davey & Smith 1992 called 'residual velocities') should represent the shift in velocity caused by the irradiated region. By taking a one-spot model to mimic the heated part, and a Roche geometry for the secondary, Davey & Smith (1992) back-projected the residual velocities on to the surface of the secondary to obtain the intensity distribution of the line. The resulting map is subsequently used to obtain a radial velocity curve, which is compared with the observed one. The process is iterated until the difference from the observed values reaches a minimum and the model and observed eccentricities match. The final output of the process is a map of the irradiated secondary and the correction needed to obtain the real semi-amplitude of the secondary star, K_2, from the observed one.

A different approach is to map the secondary star features directly (Rutten & Dhillon 1994). It is again assumed that the line being mapped arises solely from the cool star. Thus the changes in the strength and shape of the line profile in one orbit directly relate to the changes in its surface distribution on the star. However, because of the faintness of the secondary star in CVs its spectrum is usually embedded in the noise. As a result, the information on the shape of the line is essentially lost. An alternative is to use only the total line flux to create the map (Catalán et al. 1994; Davey 1994). This procedure has the advantage that it offers an extra check for the radial velocities. Its main disadvantage is that changes in the line flux, due to contamination from other areas of the binary, can create an incorrect map of the secondary star.

Both methods had been previously tested separately, and the results were very encouraging. Davey & Smith (1996) found that the maps resulting from the radial velocity deficits (i.e., the departure from circular fits), and the phase-dependent flux variations were very similar. Here we have decided to use both the radial velocity and flux information simultaneously to carry out the maps. Since the line flux measurements are less accurate, not just in the measurements themselves, but also because other regions of the binary may be affecting the line strengths, we opted to use weights on the radial velocity and flux input files. The weight of the radial velocity file was never lower than 50 per cent. It was larger for low S/N data or where the line fluxes were known to be heavily contaminated by line components originating from other areas of the binary. The values used are listed in Table 3. The weights, as such, do not have a direct bearing on the final fitting parameters summarized in Table 3. They primarily affect the combined χ^2 quoted. When fitting the data, various weights were

Table 3. Radial velocity results from mapping the line flux and residual velocities of the emission and absorption lines in QQ Vul from the secondary star. The weight of the radial velocity file used in the fit is given.

Line	Year	K_2 km s^{-1}	weight (per cent)	χ^2	position (°)	extent (per cent)
Na I 8190 Å	1991	233 ± 5	50	4	14 ± 8	43
	1993	214 ± 9	50	9	21 ± 4	32
Mg II 4481 Å	1991	169 ± 5	80	8	15 ± 4	50
	1993	135 ± 6	80	9	13 ± 2	45
He II 8236 Å	1991	101 ± 4	80	7	1 ± 6	48
	1993	66 ± 6	80	9	11 ± 3	23
C I 8335 Å	1991	122 ± 3	50	3	7 ± 1	18
	1993	80 ± 6	50	5	10 ± 3	18
Mg II 7877 Å	1991	147 ± 4	80	3	12 ± 10	32
Mg II 7896 Å	1991	147 ± 3	80	14	35 ± 11	47
Ca II 8498 Å/H I 8502 Å blend	1991	166 ± 7	50	8	24 ± 4	63
Ca II 8542 Å/H I 8545 Å blend	1991	163 ± 7	50	16	21 ± 4	64
H I 8598 Å	1991	124 ± 5	50	19	20 ± 2	50
Ca II 8662 Å/H I 8665 Å blend	1991	162 ± 5	50	15	20 ± 6	76
H I 8750 Å	1991	126 ± 1	50	48	30 ± 7	50

tried to see how much they influenced the final results. We found that significant differences existed only when the line fluxes were given all the weight. Fits solely to the flux data tended to go towards a larger binary inclination, and a more extended distribution of the line on the stellar surface.

Further changes were carried out on the original code used by Davey & Smith (1996). Instead of fixing the parameters corresponding to the mass ratio, the inclination, the mass of the secondary star and the initial guess for K_2 prior to the fits, we have modified it so that all these parameters can be freed or fixed at any time. Together with the amplitude (scalefactor), the position and the extent of the spot (cf. Davey 1994; Davey & Smith 1996), we had a code that could carry out a seven-parameter fit instead of the original three. This has the added advantage that it allowed the program to search for the lowest χ^2 by letting it vary the freed parameters itself. In this manner we could test to which parameters the fit was particularly sensitive. This was important as we did not have a complete set of parameters for QQ Vul to begin with. The final set of derived parameters is the result of an iterative process. An initial set of reasonably chosen system parameters was used to find a first estimate of the corrected K_2. This, in turn, was used to obtain a new set of parameters, which were then fed back to the fitting routine until the best fit was found. A downhill simplex method (AMOEBA; Press et al. 1988) was used to get the lowest χ^2.

Table 3 gives the radial velocity results from the surface maps. The mass ratio and the mass of the secondary star used are those that resulted from the final set of system parameters found in the next section. The χ^2 quoted are the combined reduced χ^2 of the radial velocity and flux data for each fit. Most of the lines gave smallest χ^2 for values of the binary inclination between 62° and 68°, the difference being fairly small within that range. Thus the inclination was fixed at $i = 65°$ in all the models listed. We quote only the model that resulted in the lowest combined χ^2. Also given are the position and equatorial extent of the spot on the surface of the secondary star. The position is defined as the angle measured anticlockwise from the L_1 point to the centre of the heated region, and the extent refers to the equatorial extent of the spot as a fraction of the circumference of the star (ϕ_0 and B, respectively, as defined in equation (2) in Davey & Smith 1996). The extent was constrained to lie between 0 and 80 per cent of the stellar circumference. Although we did not consider it likely for more than half of the star to be irradiated, we allowed a larger range to account for any possible redistribution of the effect of irradiation in the stellar atmosphere. In fact, all the lines mapped within 50 per cent of the stellar surface, except the Ca II/Paschen blended emission which yielded extents larger than 60 per cent. We think that the sum of a symmetric Ca II distribution covering about 50 per cent of the star with a notably asymmetric Paschen line may be the cause of this. However, an easily ionizable line such as Ca II may well just be distributed in this manner. The errors associated with the extent are less than 20 per cent, more typically about 5 per cent. The surface maps, together with the resulting model fits to the velocities and the flux values, are shown for the Na I absorption lines in Fig. 8. We also show the fit and the map for the Ca II 8542 Å/Paschen 11 blend in Fig. 9.

9 THE $v \sin i$ OF THE SECONDARY STAR

The Na I absorption lines at λ8183 and λ8194 Å were used to derive the projected rotational velocity, $v_{\rm rot} \sin i$, of the secondary star in QQ Vul. Only the high resolution spectra taken in 1993 were used for this task. Before carrying out any measuerements and in order to increase the S/N of the data, the available spectra were co-added. To avoid smearing of the lines, the shifts due to the orbital modulation of the secondary were removed, prior to the sum, as follows. Having found the spectral type of the secondary to be M4, all the red spectra were cross-correlated with a standard star spectrum of the nearest spectral type (GL 105B). With the derived shifts, the spectra were aligned and co-added. Because of the low S/N, only those that gave reasonable shifts were employed, most of which lay in the orbital phase range $\phi = 0.7 - 1.3$. These are the same ones that were used for the radial velocity determinations. Although summing over such a large phase interval is not recommended since it has the tendency to artificially broaden the lines, in this case there were no foreseeable gains from reducing the co-added range as this meant worsening the S/N.

Then the continuum of the summed spectrum and the spectral type template was removed. The template was broadened by fixed amounts using the broadening function

$$B(x) = \frac{6(1-\varepsilon)}{\pi(3-\varepsilon)}(1-x^2)^{1/2} + \frac{3\varepsilon}{2(3-\varepsilon)}(1-x^2) \qquad (4)$$

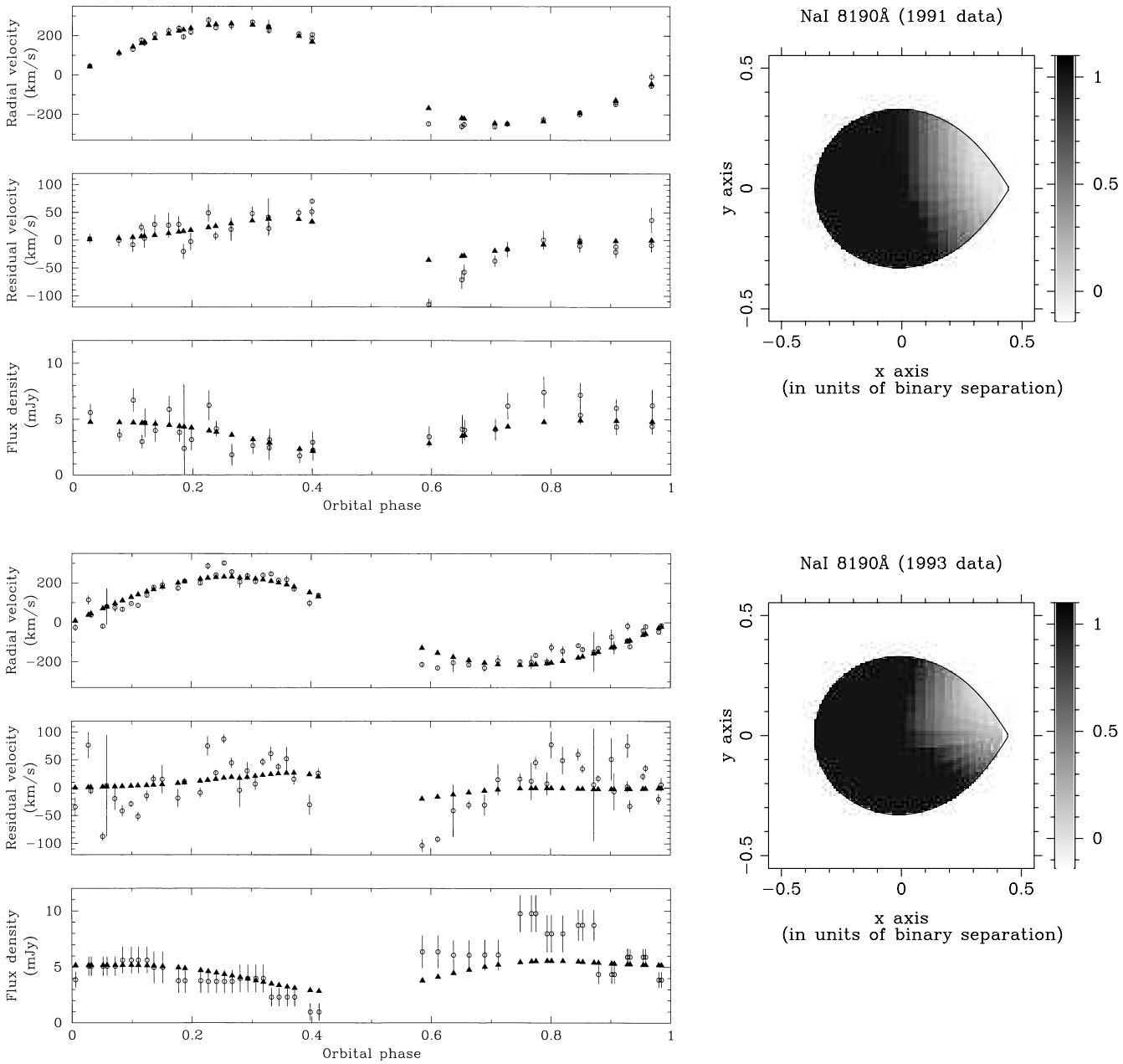

Figure 8. The Na I surface maps and the corresponding fits to the radial velocity, residual velocity and flux information. The circles represent the data, and the model fits are shown as filled triangles.

(Gray 1992), where ε is the linear limb-darkening parameter, and $x = v/v_{\rm rot} \sin i$. Using a Kurucz model atmosphere of 3500 K, Unruh (private communication) arrives at a value for the limb-darkening coefficient of ~ 0.36 for $\lambda 8000$ Å. We used this value for the limb darkening. The broadened spectra were then scaled to the averaged QQ Vul spectrum. The smallest χ^2 was found for $v_{\rm rot} \sin i = 110 \pm 15\,{\rm km\,s^{-1}}$. The fit is shown in Fig. 10.

10 DETERMINATION OF THE SYSTEM PARAMETERS AND DISCUSSION

10.1 The eccentricity problem and correcting the observed K_2

It is immediately obvious that the results from the surface maps do not yield a single value of the 'true' K_2 of the secondary star (Table 3). In fact, even for the same line the so-called 'corrected' K_2 is different for the two epochs. Of particular interest are the velocities of the Na I doublet near 8190 Å because of the lines' pivotal role in parameter determination. In a previous study of QQ Vul by Mukai & Charles (1987), corresponding to the first detection of the Na I lines in this object, they found that the radial velocity semi-amplitude of the secondary star is $209 \pm 28\,{\rm km\,s^{-1}}$. Our measurements yield semi-amplitudes of $271 \pm 3\,{\rm km\,s^{-1}}$ (1991) and $228 \pm 2\,{\rm km\,s^{-1}}$ from the circular fits, with corresponding corrected velocities of 233 ± 5 and $214 \pm 9\,{\rm km\,s^{-1}}$, respectively. What *is* the true K_2 of the secondary star in QQ Vul?

The real question here is how one should interpret the values of eccentricity obtained from the elliptical fits. As mentioned earlier, a star in a circular orbit around the centre of mass of the system, is

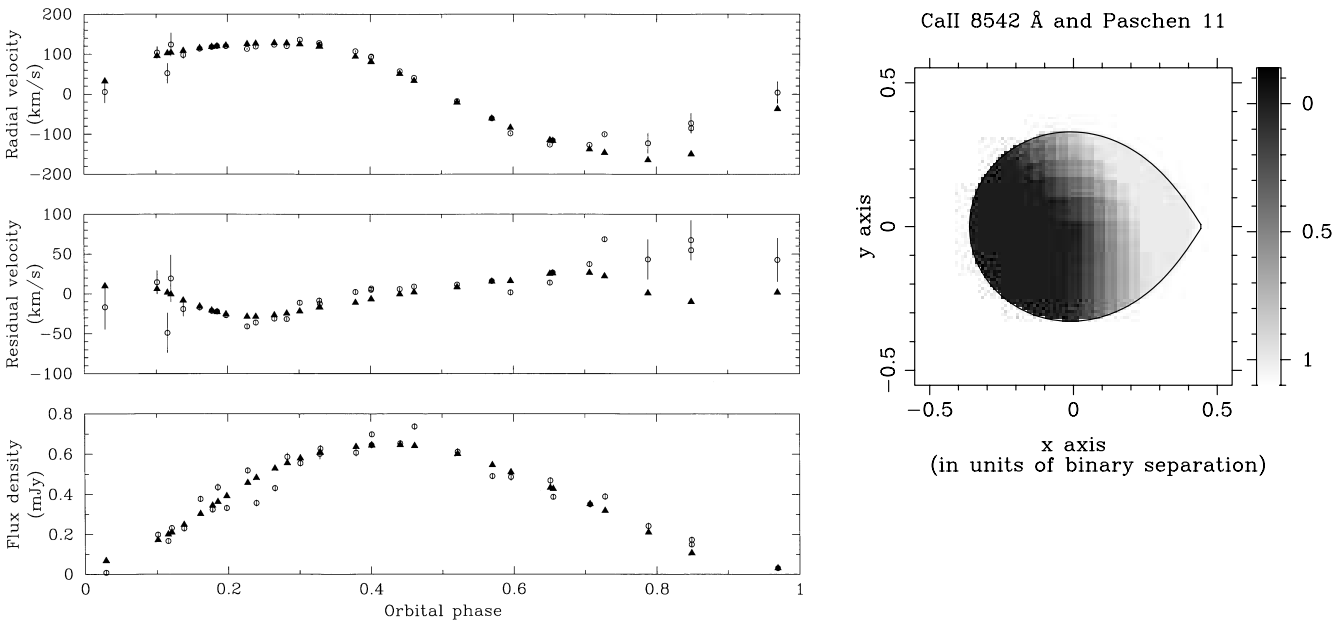

Figure 9. Intensity map of the Ca II 8542-Å line and Paschen 11 blend with the corresponding fits to the radial velocities, the residual velocities and the emission-line flux variations. The circles are the observed velocities and the filled triangles are the model fits.

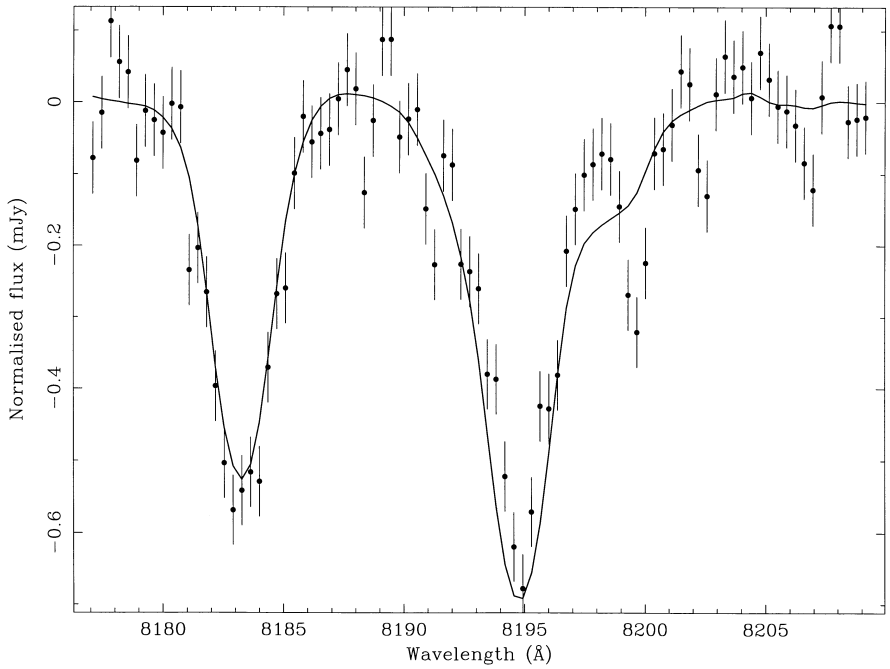

Figure 10. The co-added far-red spectrum of QQ Vul (filled circles) shown with the best-fitting rotationally broadened spectrum (solid line).

expected to exhibit a slightly elliptical radial velocity variation if the distribution of the line over the stellar surface is limited to a region of the star. It follows that if Na I on a late-type secondary star is somehow depleted in the hemisphere facing the white dwarf, perhaps due to irradiation, then not only will the resulting K_2 be larger, but also the line velocities will show a significant eccentricity. This is what Martin (1988) found in her study of IP Peg. By modelling a symmetrically heated (relative to L_1) Roche-shaped star and assuming that the eccentricity is entirely due to high levels of irradiation, Martin found that the correction to the observed K_2, using the Na I doublet in the far-red, can be as much as 20 per cent (see fig. 2 in Davey & Smith 1992). In this model the correction necessary to obtain the true value of K_2 is essentially directly proportional to the amount of eccentricity detected. However, if we apply this idea to our derived eccentricities, we obtain an incorrect result. If the above were true, one would expect to find a higher eccentricity for the larger observed K_2, i.e., in the 1991 data set. What we observe is just the contrary. The 1993 data, where the secondary appears less irradiated and the observed K_2 is smaller, actually gives the larger eccentricity. Thus the eccentricity, on its own, is not a good measure of the degree of depletion of the Na I in the illuminated face of the red dwarf, and does not necessarily reflect the amount of correction needed to find the true K_2 from the observed one.

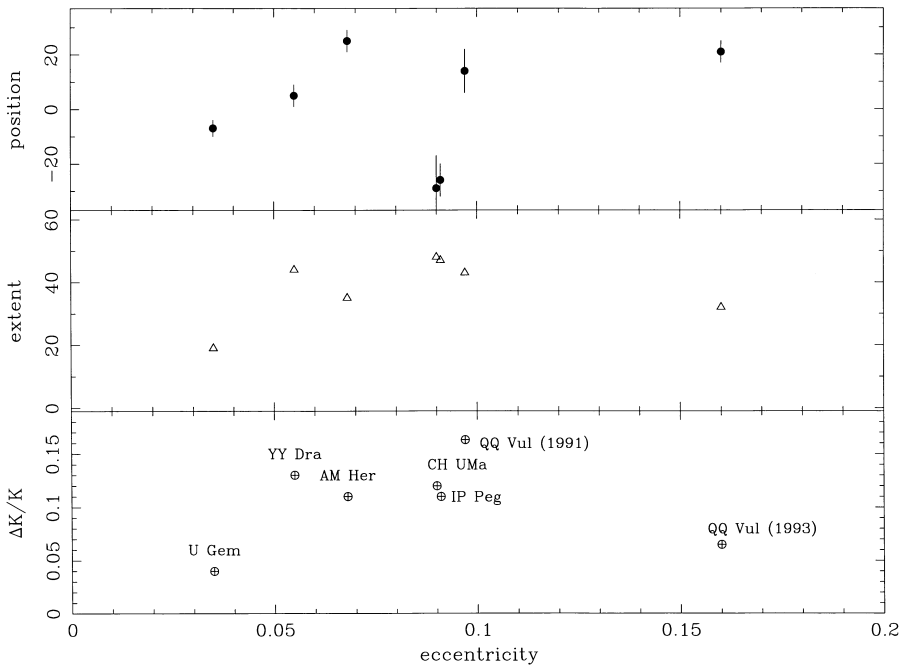

Figure 11. Plot of $\Delta K/K_2$, position and extent of the spot against the eccentricity of the radial velocity curve based on the results from Davey (1994). $\Delta K/K_2$ is the relative amount by which the measured semi-amplitude has increased due to off-centred irradiation. The points are labelled with their corresponding objects. Also shown are the results for QQ Vul from this study.

In his study of the Na I surface distribution in CV secondaries, Davey (1994) found that the effect of an *asymmetric* irradiation distribution could lead to quite a high eccentricity in the radial velocity curve, but not necessarily imply a large correction to the observed K_2. To see whether this applies to QQ Vul, we have plotted in Fig. 11 Davey's results against eccentricity for the five objects included in his analysis and the ones we obtained from QQ Vul. We find that, although an asymmetric heating distribution may play a part, it is not entirely successful in explaining our results for QQ Vul. For the 1991 spectra, where the secondary is almost certainly very irradiated, the predicted correction to K_2 follows the trend shown by the other objects. However, the corresponding ΔK_2 is too small. The corrected K_2 for 1991 barely matches the observed K_2 in 1993 (prior to any corrections). Since the maps resulting from the 1993 spectra indicate that some heating was also present then, the observed K_2 for 1993 would also require a correction, widening the gap between the final K_2 values even further, contrary to what one would expect. Furthermore, the extremely large eccentricity resulting from the 1993 data does not even fall in the general increasing trend (against eccentricity) shown by all the other points in Fig. 11. Therefore the proposed direct relationship between the amount of eccentricity and irradiation (Martin 1988), even if one takes into account the possibility of an asymmetric surface distribution of the line (Davey & Smith 1992), is at best only true for intermediate values of eccentricity ($e \leq 0.1$).

We considered whether the eccentricities may be attributed to effects external to the red dwarf. For example, large observational errors may be partially to blame. Lucy & Sweeney (1971) found that observational errors alone can mount up false eccentricities of up to 0.03. Another possible (and related) cause is contamination of the Na I lines by the nearby He II and Paschen jump from the stream. To investigate this avenue,we have modelled what effect a broad stream component from the He II 8236-Å line and the Paschen jump could do to the Na I velocities. We found that this can result in eccentricities of up to 0.03, but not more. Thus, at most, we can account for $e \approx 0.06$. The errors in the 1993 data set are, on the whole, larger than in the 1991 data as a result of the higher resolution and shorter exposures. If heating was also much less, as indicated by the maps, then the contribution of the stream component to the lines would be more dominant. Therefore contamination of our derived velocities by the stream component is more likely. If we assume that both effects were present in the 1993 spectra, then the eccentricity would be reduced to about the same level as in 1991: $e \approx 0.1$. This is still higher than is expected from the model fits, since the degree of heating was less in 1993 than in 1991.

This and the fact that both the velocity and flux surface mapping give poor fits seem to suggest that what we are seeing may truly be caused by a more complex distribution of the Na I lines on the secondary star surface, the models being too simple to be able to account for them. There must be other causes for the extra eccentricity (or the radial velocity curve's deviation from circular) in addition to any existing irradiation and its asymmetric distribution on the stellar surface, which is present even when the red dwarf is weakly illuminated.

A non-homogeneous distribution of Na I on the stellar surface could create false eccentricities independent of any irradiation or heating mechanism on the star. The QQ Vul Doppler maps corresponding to the Na I line in 1993 show marginal signs of a non-uniform distribution. The high rotation rate of the red dwarf in QQ Vul and the fact that it is already somewhat embedded in the strong field of the white dwarf almost certainly suggest the presence of a strong field on the secondary. Given our current understanding of magnetic activity, starspots and their relationship to convection and rotation, it is very likely that starspots are present on the surface of the red dwarf. The cool component in RS CVn stars, which are similar in spectral type to the red dwarf in QQ Vul and are rapidly rotating, have long been known to harbour starspots (Baliunas & Vaughan 1985). These spots produce

distortions in the stellar profiles that would result in radial velocity variations (Hatzes 1999). Changes in the the local magnetic configuration of the white dwarf in QQ Vul, or perhaps magnetic activity cycles on the secondary, could create time-dependent starspot distributions (from epoch to epoch) which would have a direct effect on the observed eccentricities.

The above, coupled with the presence of some irradiation, noisy data and contamination from the stream, could end up giving large eccentricities, but not necessarily a large correction to the derived value of K_2. Therefore the original suggestion by Martin (1988) that the amount of eccentricity essentially represents the degree of heating is not generally true. This also implies that the true uncertainties in the results from the surface maps are very likely to be much larger (50 per cent or more) than the originally quoted values. The only way to obtain an accurate measurement of the true K_2 is by having a large enough data set, taken at separate intervals over a long time baseline. This way any temporal changes of the line distribution are taken into account. However, it still stands that if irradiation is prevalent on the star, then the derived velocities have to be corrected for this effect. So far, the best way of doing this is by using a surface map model and preferentially one with a photospheric line from the secondary star.

From the 1991, 1993 and Mukai & Charles (1987) circular radial velocity fits, and taking into account the errors on each measurement, K_2 must satisfy $208 \leq K_2/\mathrm{km\,s^{-1}} \leq 264$. There is no doubt that the secondary star was significantly irradiated in 1991. If as much as half of the star was depleted of Na I, then, based on the expression derived by Wade & Horne (1988) for the maximum '*K*-correction', the observed K_2 could be as much as $49\,\mathrm{km\,s^{-1}}$ larger than the true value. In other words, for the 1991 data alone, the lowest possible semi-amplitude for the secondary is $K_2 = 222\,\mathrm{km\,s^{-1}}$. From the surface maps we find that for the same data $K_2 = 233 \pm 5\,\mathrm{km\,s^{-1}}$ for an extent of 43 per cent of the irradiated surface. Since it is possible that up to half of the star was irradiated, we will adopt more conservative errors. Thus $K_2 = 233 \pm 14\,\mathrm{km\,s^{-1}}$ in 1991. In 1993 the extent of the Na I depletion is much smaller, being absent only in the region near L_1. From the surface map fits we derive $K_2 = 214 \pm 9\,\mathrm{km\,s^{-1}}$ for irradiation affecting 32 per cent of the stellar surface. Based on nine points, Mukai & Charles (1987) find an even smaller K_2, suggesting that the amount of heating was even less or none at all when their observations were taken in 1985. On the face of it, if irradiation is the sole cause of the larger K_2, then the value found by Mukai & Charles must be the nearest to the true K_2. If, however, other effects have some bearing on the line distribution even when the secondary is not irradiated (such as surface element abundance anomalies or starspots), then it would be wrong to discriminate between any of the results so far. Thus we have opted to take the weighted mean (weighted according to the errors) of our corrected values and that found by Mukai & Charles. We find that the most likely semi-amplitude of the radial velocity of the secondary star is $K_2 = 219 \pm 6\,\mathrm{km\,s^{-1}}$.

10.2 K_2 from the emission lines

Since the secondary stars are usually difficult to detect in short-period binaries such as AM Her stars, it is common practice to employ the narrow-emission-line radial velocities, believed to originate from the heated regions of the red dwarf, to derive the true K_2 and subsequently estimate the rest of the binary parameters. It is usually assumed that the emission arises on the surface of the red dwarf. Thus the observed K_2 is smaller than the true K_2 by an amount which depends primarily on the distribution of the line and has to be corrected. For fixed parameters of the irradiation model, a relationship between q and K_{obs}/K_2 can be found (Beuermann & Thomas 1990), making it possible to derive the range of q and i (Paper II).

The semi-amplitude of the radial velocities of the emission lines from the irradiated hemisphere of the red dwarf in QQ Vul varies between 53 and $150\,\mathrm{km\,s^{-1}}$ in the 1991 and 1993 data sets. The emission lines that showed surface coverages larger than about 40 per cent of the star had semi-amplitudes $K_2 > 100\,\mathrm{km\,s^{-1}}$, while those which were primarily concentrated near the L_1 point had velocities of less than $100\,\mathrm{km\,s^{-1}}$. Assuming that the narrow emission lines are located on the secondary star chromosphere, the surface maps should, in principle, produce the corrected values for the observed K_2 as dictated by the radial velocity and flux variations in phase. The resulting K_2 ought to match the corrected value calculated from the non-irradiated hemisphere within the errors imposed by the quality of the data set. With this in mind and as a check, we calculated the emission-line surface maps.

Our results are summarized in Table 3. As can be seen, at best even the largest of the corrected values are smaller by about $50\,\mathrm{km\,s^{-1}}$ than our average K_2 (from the Na I). In the case of the He II lines, the corrected K_2 is smaller by more than $150\,\mathrm{km\,s^{-1}}$. It is not clear why such large discrepancies exist in the derived velocities between the absorption and emission lines. Contamination from the stream component could be partially to blame (cf. Martin et al. 1989), although it is usually quite distinct and a lot of care has been taken to minimize its effect. Another possibility is that the lines are reprocessed in some kind of cloud located near the L_1 point, or more likely on the upper layers of the red dwarf chromosphere (which is not included in the surface mapping model). The Doppler map of the C I in the 1993 data does show that the peak of the emission occurs somewhere between the L_1 point and the binary centre of mass, with very little flux actually overlapping with the limits of the secondary star in velocity space. The emission from He II and Mg II also extend far beyond the limits of the secondary surface. The problem with this suggestion is that the differences in velocity are a significant fraction of the stellar radius, implying a location in the stellar corona rather than the chromosphere. One could speculate that if the secondary in QQ Vul turns out to show magnetically related phenomena, then prominence-like structures may exist in the region of the L_1 point which could be irradiated by the high X-ray emission and hence emit. After all, the conditions in very irradiated red dwarfs in magnetic CVs are rather unusual in comparison to single active M-dwarf stars. However, with no detailed models there is no way of knowing.

There are also large ranges in the velocities derived from the various emission lines. While the Mg II and the Ca II/Paschen blends give similar velocities, they differ by nearly $70\,\mathrm{km\,s^{-1}}$ from the He II line. It is possible that the differences in the velocities between the lines may relate to different layers of the red dwarf's chromosphere, with helium and carbon being ionized much higher up (nearer to the irradiating source), and Ca II and H I being reprocessed much nearer the stellar surface. Thus the deeper the lines are in the chromosphere the better will the estimate of K_2 be. However, regardless of whether the above suggestion is correct or not, the large range of K_2 values found indicates that care has to be taken when interpreting the stellar dimensions derived from the velocities of the emission lines from the secondary star.

10.3 The systemic velocity of the spectral lines in QQ Vul

Quite a number of lines both emission and absorption originating from the secondary star indicate that the systemic velocity of QQ Vul is consistent with being zero (Tables 1 and 2). Perhaps the best indicators of this are the Na I lines, which are photospheric lines. The He II, Ca II and C I lines also give tiny deviations of γ from zero. We suspect that these deviations from zero are a result of a slightly non-random scatter in the points, possibly caused by contamination from other regions of the binary. For example, the Ca II triplet are blended with the nearby Paschen emission lines which not only have a strong stream component but also exhibit an asymmetric distribution on the red dwarf. Therefore previous estimates yielding large systemic velocities, as high as $500\,\mathrm{km\,s^{-1}}$ (Nousek et al. 1984; Osborne et al. 1987) in some cases, are likely to be the result of lower resolution spectra and the fact that the velocities were obtained from fitting the three-component emission lines as a single Gaussian. Any changes in the stream configuration may lead to changes in our viewing angle of the stream. It is not unlikely that at any given time we may be detecting the stream infall velocities more than at others, and thus getting much larger γ velocities.

However, the Mg II and the Paschen emission lines do show γ velocities which are significantly different from zero. These velocities average out to $-28 \pm 8\,\mathrm{km\,s^{-1}}$ in the 1991 data. Although it is not possible to ascertain whether the 1993 data also showed this trend because of the narrower spectral range covered, the γ velocity for the Mg II 4481-Å line is consistent with the negative values derived in 1991. These are also much the same as the ones found by Mukai et al. (1986).

10.4 Asymmetric heating on the secondary star

One of the prime reasons for observing QQ Vul was to see whether the Na I lines have an asymmetric heating distribution, similar to that found in AM Her (Southwell et al. 1995; Davey & Smith 1996), with the irradiation spot located in the trailing edge of the star. Davey & Smith (1992) found that all the discal CVs included in their study showed a preferred asymmetry towards the leading edge. Although at the time of our observations there were no other magnetic systems known to have an asymmetric heating distribution on the secondary, a Doppler map analysis of the emission lines in HU Aqr carried out at a later date by Schwope, Mantel & Horne (1997) showed that it too was asymmetrically heated in the same way as AM Her. Thus there was a strong possibility that the red dwarf in QQ Vul, and maybe even in all polars, exhibited this kind of heating distribution.

Our results from both the Doppler and surface maps of QQ Vul show that the distribution of the Na I line is asymmetric, and that the irradiated region is preferentially distributed towards the following edge of the red dwarf. In addition, we find that the asymmetries were more pronounced in 1993 when the secondary appeared to be less irradiated. However, we also find that within the same epoch the degree of the asymmetry is somewhat line-dependent. While the H I, Na I and Mg II lines exhibit a marked asymmetric distribution in both the Doppler and the surface maps, the far-red He II and C I emission lines do not. In fact, their distribution is consistent with being symmetric relative to the L_1 point for the 1991 data set. The asymmetry in the Ca II triplet in the 1991 spectra is more uncertain. Although the Doppler maps show a fairly symmetric distribution of the lines in velocity space, the best surface map models yield significant asymmetries. The irradiation spot is preferentially located between 14° and 29° from the line of centres. It is possible that the asymmetry detected in the Ca II is caused by the underlying Paschen lines. However, because the lines are blended, we cannot rule out that what we detect is intrinsic to the Ca II triplet. What we do find from the surface maps is that the velocities are not well modelled between phases $\phi = 0.7$ and 0.9 in all the Paschen lines, particularly those blended with Ca II, i.e., at the same phases where the Na I fits also fail. This suggests that whatever it is that might be contaminating the Ca II lines in that phase region might also be affecting the Na I absorption lines.

How such large asymmetries come about is not well understood. Martin & Davey (1995) found that the combined effect of heating and Coriolis forces can induce atmospheric motions on a thin surface layer of a rapidly rotating star. This can cause the heating to be preferentially distributed towards the leading side of the red dwarf. Thus the asymmetry seen in the irradiated secondaries of CVs with a disc could be associated with the presence of such atmospheric motions. However, it is not immediately evident why the same process is not manifested in the secondary stars of the polars studied to date. One suggestion is that, as the heating source in AM Hers is located on the white dwarf surface, asymmetric heating is possible if absorbing matter is between the irradiating source and the secondary star. The idea is that the accretion curtain, associated with the magnetic structure of the white dwarf, partially shields the red dwarf from the X-ray flux (Southwell et al. 1995; Davey & Smith 1996; Schwope et al. 1997). If this is the correct scenario, then the differences in the heating distribution between the two epochs may be attributed to a change in the mass transfer rate, on to a shift in the position of the X-ray-emitting pole relative to the line of centres, or to variations on the red dwarf atmosphere intrinsic to the star. In the case of the first suggestion, at times of high mass transfer rate more UV flux will be available to go through the accretion stream and reach the red dwarf, creating a less asymmetric heating pattern. This would explain why there are larger asymmetries when the secondary appears less irradiated, at least in the case of QQ Vul. The second possibility is that a change in the position of the accreting pole will lead to a change in the position of the accretion curtain, associated with the magnetic field, relative to the red dwarf, thus exposing it more (or less) to the X-ray emission from the white dwarf. Finally, it is also possible that the changes in emission and absorption line distribution are entirely intrinsic to the red dwarf if it turned out to be very magnetically active. Hence the changes seen may be due to magnetically induced atmospheric variations leading, for example, to the presence of large starspot regions on the star. With our data set and from our results it is not possible to tell which of these ideas may apply. However, if the asymmetries turn out to be caused by the system geometry, then the maps could prove to be a good way of probing the magnetic configuration and temperature of the white dwarf and accretion column.

10.5 Revised binary parameters for QQ Vul

With our derived values of the projected rotational velocity of the secondary star, $v_{\rm rot}\sin i$, and the K_2 velocity from the Na I doublet we find that

$$\frac{v_{\rm rot}\sin i}{K_2} = (1+q)f(q) = 0.50 \pm 0.08, \qquad (5)$$

where $f(q)$ is the expression from Eggleton (1983). Therefore the mass ratio of QQ Vul is $q = 0.54 \pm 0.14$.

Using the empirical mass–radius relationship found by Caillault & Patterson (1990), the rotational velocity of the absorption lines is given by

$$v_{\rm rot} = 119.4\, P^{0.1469} f^3(q) \left(\frac{1+q}{q}\right)^{0.574} \quad (6)$$

for secondary star masses less than about $0.5\,{\rm M}_\odot$, where P is in seconds and $v_{\rm rot}$ in $\rm km\,s^{-1}$. Together with our derived $v_{\rm rot}\sin i$, we estimate a binary inclination of $i = 59^{+17}_{-12}{}^\circ$. The large errors result from the large uncertainties in q. This range for i is essentially the same one found by Nousek et al. (1984). However, it is possible to narrow down this range further. Based on the surface maps, the best fits were obtained for a binary inclination of $i = 65^\circ \pm 7^\circ$, with lowest χ^2 found for values of i between 62° and 68°, in all the lines studied (both emission and absorption) originating on the red dwarf. This value is in good agreement with the above estimate and previous estimates made by Nousek et al. (1984) and Mukai & Charles (1987) from spectroscopy, but it is larger that the one deduced by Cropper (1998) from polarimetry.

The mass of the primary star can be found from

$$M_1 = \frac{PK_2^3(1+q)^2}{2\pi G \sin^3 i}. \quad (7)$$

For i in the range 58°–72°, we derive a primary star mass of $M_1 = 0.54^{+0.21}_{-0.16}\,{\rm M}_\odot$. This is half the mass estimated by Cropper, Ramsay & Wu (1998) from *Ginga* data using a modified warm absorber and the multitemperature bremsstrahlung model. Using our derived q, we obtain a mass for the secondary star of $M_2 = 0.30 \pm 0.10\,{\rm M}_\odot$. Our calculated M_2 is smaller by about 11 per cent than the secondary star mass resulting from the mass–period relationship derived from Caillaut & Patterson (1990) (although it is within the errors of their empirical fit), but at the higher end of the mass range allowed by its spectral type (Kirkpatrick & McCarthy 1994). Using the mass–radius relationship in Caillault & Patterson (1990), we obtain a radius for the secondary of $R_2 = 0.35 \pm 0.10\,{\rm R}_\odot$. Based on all the above parameters, we calculate a binary separation of $a = 1.14 \pm 0.12\,{\rm R}_\odot$ and a likely radial velocity semi-amplitude of the white dwarf primary of about $120\,\rm km\,s^{-1}$. The derived binary parameters are listed in Table 4.

We are fairly confident that our inferred i from the surface maps is reliable for a number of reasons, other than the fact that all the surface fits favour it. First of all, the H I, Mg II and Ca II emission lines originating from the heated face of the secondary and stream have zero flux near binary phase $\phi = 0$, which indicates that $i > 50^\circ$ as already suggested by Mukai & Charles (1987). More importantly, not only do we see a sharp decrease in continuum flux at phase zero at practically all wavelengths at which QQ Vul has been observed in the past (Nousek et al. 1984; Mukai et al. 1986; Osborne et al. 1986; Mukai et al. 1986; Mukai & Charles 1987; Cropper 1998), but also most of the emission lines are almost totally eclipsed at this phase (Paper II), indicating that the primary source of both the continuum and line fluxes are occulted when the secondary is in our line of sight. The same behaviour of the continuum and lines was already noted by Nousek et al. (1984) and Mukai et al. (1986). In fact, the idea that i must be at the higher end of the possible range was already suggested by Nousek et al. based on the cyclotron glitch they detected near inferior conjunction of the red dwarf.

Table 4. Binary parameters of QQ Vul derived using the Na I absorption lines.

Binary separation a	$1.14 \pm 0.12\,{\rm R}_\odot$
Inclination i	$65 \pm 7^\circ$
Mass ratio $q = M_1/M_2$	0.54 ± 0.08
Primary star mass M_1	$0.54^{+0.21}_{-0.16}\,{\rm M}_\odot$
Secondary star mass M_2	$0.30 \pm 0.10\,{\rm M}_\odot$
Secondary star radius R_2	$0.35 \pm 0.10\,{\rm R}_\odot$
Velocity semi-amplitude of the secondary K_2	$219 \pm 6\,\rm km\,s^{-1}$
Projected rotational velocity of the secondary $v_{\rm rot}\sin i$	$110 \pm 15\,\rm km\,s^{-1}$

Because the shape and exact position of the continuum and flux dip vary in time, and since the lines are not always totally eclipsed, we do not think that the white dwarf is eclipsed in QQ Vul. This provides us with an upper limit for i, which we estimate to be about $i = 72^\circ$ for $q = 0.54$. A large fraction of the outer edges of the dip must be due to a self-occultation of the accretion stream. The position corresponding to minimum flux does not vary more than 0.05 of a binary phase relative to phase zero. Since there is evidence that the emission lines in QQ Vul do not always show the same behaviour [e.g., the He II emission line had almost constant flux in 1984 (Mukai et al. 1986)], we tentatively suggest that the changes can be attributed to small variations in the magnetic configuration of the white dwarf, leading to shifts in the position of the stream and accretion column relative to the line of centres as suggested in Catalán et al. (1994).

11 CONCLUSIONS

Using high- and medium-resolution spectroscopy taken in 1991 and 1993, we have carried out an exhaustive analysis of the far-red spectra of the magnetic CV QQ Vul. In addition to the Na I absorption doublet at 8190 Å, we have identified the presence in emission of Mg II at 4481, 7877 and 7896 Å, He II at 8236 Å, C I at 8335 Å, and re-confirm the presence of the Paschen and Ca II triplet emission lines detected by Mukai & Charles (1987). As previously suspected by McCarthy et al. (1986) and Mukai & Charles (1987), we found that most of the emission lines seen in the far-red have a prominent narrow component which follows the movement of the secondary star.

Equipped with low-resolution spectra covering the TiO bands in the red, we have classified the secondary star to be M4V to better than a spectral type. The velocities and fluxes of all the lines known or suspected to originate from the donor star were measured. The radial velocities of the Na I doublet in the 1991 and 1993 data sets were calculated using a cross-correlation with a template spectrum. For the 1991 data the template employed was a synthetic spectrum, while for the 1993 data an M4.5V spectral type standard star spectrum was used. Double-Gaussian absorption profiles were employed to obtain the Na I line fluxes. Single-Gaussian fits to the narrow-emission-line component of all the lines present in the spectrum were used to derive the emission-line velocities and fluxes. The results of the circular fits to the radial velocity curves are summarized in Table 1.

To study the location of the emission and absorption lines, we employed both Doppler (Marsh & Horne 1988) and surface mapping (Davey & Smith 1992) techniques. The maps confirm that the emission arises on the side of the red dwarf directly facing the white dwarf. We interpret this as due to light from the white

dwarf and accretion column reprocessed by the secondary star. We also found that some of the emission lines – the ones with higher ionization potentials – are primarily located in a small area above the L_1 point. Because of the rather small velocities found in some of these lines, we tentatively suggest that the ionized gas might be located at high levels of the red dwarf chromosphere, around L_1. It is possible that the differences in the velocities correspond to different depths in the stellar atmosphere with the lower ionization potential lines such as H I, Mg II and Ca II still being easily ionized at larger depths. This, combined with contamination of the line velocities and flux by the stream component, would explain why the surface maps fail to correct the observed emission-line velocities to match the ones from the Na I photospheric lines. If the emission lines do form in an extended chromosphere of the red dwarf, then care should be taken when interpreting the mass determinations resulting from their K velocities.

The extent of the emission and absorption on the secondary were found to be different in the two data sets suggesting that the degree of heating is variable. As the source of the EUV light must be the accretion regions near or on the white dwarf, we suggest that the variations seen on the secondary reflect the changes in the accretion on to the white dwarf. Such a dependence has been found by Somers & Naylor (1999) to exist in an old nova.

An asymmetric distribution of the Na I lines, similar to the one found in AM Her and the emission lines in HU Aqr, was found in QQ Vul. The region of Na I depletion was preferentially distributed towards the trailing edge of the red dwarf. The same configuration was found for the Mg II and H I emission lines in both data sets. However, the degree of the asymmetry was different in the two data sets, with the larger asymmetries seen in 1993 when heating from the white dwarf appeared to be less. In contrast, it appears likely that the Ca II triplet are symmetrically distributed relative to the line of centres; the asymmetry in the surface map possibly caused by the contaminating Paschen line. We conclude that asymmetries are not only line-dependent but also change in time.

The surface maps of the Na I line have been used to find the extent of the line and the necessary correction to the observed value of K_2. We have found that the models did not give totally satisfactory fits to the velocities and line fluxes between orbital phases $\phi = 0.6$ and 0.8. We propose that these discrepancies and the large eccentricities may be caused by the presence of starspots. We conclude that the direct relationship suggested by Martin et al. (1989) between the amount of the eccentricity found in the fit of the radial velocity curve and the degree of correction necessary is generally not true. This relationship fails even when taking into account the presence of asymmetries in the line distribution. Therefore the corrections resulting from the surface maps are not as accurate as initially thought (Davey 1994). We have estimated the K velocity of the secondary from an average of the corrected values for our two epochs and using the result from Mukai & Charles (1987). We find that $K_2 = 219 \pm 6\,\mathrm{km\,s^{-1}}$.

The co-added spectrum of the high-resolution data was used to derive the projected rotation velocity of the red dwarf. Our fit to the Na I lines shows that $v_{\rm rot} \sin i = 110 \pm 15\,\mathrm{km\,s^{-1}}$. Together with the corrected K_2 velocity of the Na I lines, we derive a mass ratio of $q = 0.54 \pm 0.14$. Based on the best fits obtained from the surface maps, the narrow-emission-line flux variations from the heated face of the secondary, the continuum changes and flux variations of all the prominent lines in the blue spectra, we estimate that the inclination of QQ Vul is $65° \pm 7°$. From this we were able to determine estimates of the masses and other binary parameters. These are collated in Table 4. We stress that these results assume that it is valid simply to average the corrected values of K_2; since we do not understand why the corrected values are so different, this procedure may not be valid, and the results should be used with caution.

ACKNOWLEDGMENTS

We thank Stephen Davey for providing us with a copy of the surface mapping program RADMAP and Tom Marsh for the use of DOPPLER and the data reduction and analysis package MOLLY. We express our gratitude to Derek Jones for helping with the 1993 observations. We also thank Danny Steeghs for the tutorial on DOPPLER, Rob Jeffries, Barry Smalley and the referee for invaluable information on activity in cool stars and stellar atmospheres, and Andy Beardmore, Janet Wood and Greg Beekman for discussions. We acknowledge the data reduction and analysis facilities provided by the Starlink Project which is run by CCLRC on behalf of PPARC at the Sussex, St Andrews and Keele nodes. The William Herschel Telescope is operated by the ING at the Observatorio del Roque de los Muchachos of the Instituto de Astrofísica de Canarias. MSC was supported by a PPARC postdoctoral grant for part of this work.

REFERENCES

Baliunas S. L., Vaughan A. H., 1985, ARA&A, 23, 379
Beardmore A. P., Ramsay G., Osborne J. P., Mason K. O., Nousek J. A., Baluta C., 1995, MNRAS, 273, 742
Beuermann K., Thomas H. C., 1990, A&A, 230, 326
Caillault J.-P., Patterson J., 1990, AJ, 100, 825
Catalán M. S., Davey S. C., Sarna M. J., Smith R. C., Wood J. H., 1994, MNRAS, 269, 879
Catalán M. S., Sarna M. J., Jomaron C. M., Smith R. C., 1995, MNRAS, 275, 153
Catalán M. S., Davey S. C., Smith R. C., Jones D. H. P., 1996, in Evans A., Wood J. H., eds, Cataclysmic Variables and Related Objects. Kluwer, Dordrecht, p. 227
Cropper M., 1998, MNRAS, 295, 353
Cropper M., Ramsay G., Wu K. W., 1998, MNRAS, 293, 222
Davey S. C., 1994, DPhil thesis, Univ. Sussex, Falmer, Brighton
Davey S. C., Smith R. C., 1992, MNRAS, 257, 476
Davey S. C., Smith R. C., 1996, MNRAS, 280, 481
Dhillon V. S., 1990, DPhil thesis, Univ. Sussex, Falmer, Brighton
Drew J. E., Jones D. H. P., Woods J. A., 1993, MNRAS, 260, 803
Eggleton P. P., 1983, ApJ, 268, 368
Friend M. T., Martin J. S., Smith R. C., Jones D. H. P., 1990a, MNRAS, 246, 637
Friend M. T., Martin J. S., Smith R. C., Jones D. H. P., 1990b, MNRAS, 246, 654
Gliese W., 1969, Catalogue of Nearby Stars. Veröff. Astron. Rechen-Inst. Heidelberg, Nr. 22
Gray D. F., 1992, The Observation and Analysis of Stellar Photospheres. Cambridge Univ. Press, Cambridge
Hatzes A., 1999, in Hearnshaw J. B., Scarfe C. D., eds, Precise Stellar Radial Velocities, ASP Conf. Ser. Vol. 185, Proc. IAU Colloq. 170. Astron. Soc. Pac., San Francisco, in press
Horne K., 1986, PASP, 98, 609
Joy A. H., 1954, ApJ, 120, 377
Kaitchuck R. H., Schlegel E. M., Honeycutt R. K., Horne K., Marsh T. R., White II J. C., Mansperger C. S., 1994, ApJS, 93, 519
Kirkpatrick J. D., McCarthy D. W., 1994, AJ, 107, 333
Lucy L. B., Sweeney M. A., 1971, AJ, 76, 544
Marsh T. R., 1988, MNRAS, 231, 1117
Marsh T. R., Horne K., 1988, MNRAS, 235, 269

Martin T. J., Davey S. C., 1995, MNRAS, 275, 31
Martin J. S., 1988, DPhil thesis, Univ. Sussex, Falmer, Brighton
Martin J. S., Jones D. H. P., Smith R. C., 1987, MNRAS, 224, 1031
Martin J. S., Friend M. T., Smith R. C., Jones D., 1989, MNRAS, 240, 519
McCarthy P., Bowyer S., Clarke J. T., 1986, ApJ, 311, 873
Mukai K., Charles P. A., 1987, MNRAS, 226, 209
Mukai K. et al., 1986, MNRAS, 221, 839
Nousek J. A. et al., 1984, ApJ, 277, 682
Nugent J. J., 1983, ApJS, 51, 1
Osborne J. P. et al., 1986, MNRAS, 221, 823
Osborne J. P., Beuermann K., Charles P. A., Maraschi L., Mukai K., Treves A., 1987, ApJ, 315, L123
Press W. H., Flannery B. P., Teukolsky S. A., Vetterling W. T., 1988, Numerical Recipes. Cambridge Univ. Press, Cambridge
Rutten R. G. M., Dhillon V. S., 1994, A&A, 288, 773
Schwope A. D., 1991, PhD thesis, Technical Univ. Berlin
Schwope A. D., Mantel K.-H., Horne K., 1997, A&A, 319, 894
Schwope A. D. et al., 1998, in Howell S., Kuulkers E., Woodward C., eds, Wild Stars in the Old West: Proceedings of the 13th North American Workshop on Cataclysmic Variables and Related Objects. Astron. Soc. Pac., San Francisco, p. 44
Schwope A. D., Beuermann K., Catalán M. S., Metzner A., Steeghs D., Smith R. C., 1999, MNRAS, accepted (Paper II)
Shortridge K., 1991, FIGARO 3.0–General Data Reduction and Analysis. Starlink Project, Rutherford Appleton Lab., SERC
Smart W. M., 1977, Textbook on Spherical Astronomy, Cambridge Univ. Press, Cambridge
Smith R. C., Sarna M. J., Catalán M. S., Jones D. H. P., 1997, MNRAS, 287, 271
Somers M. W., Naylor T., 1999, MNRAS, submitted
Southwell K. A., Still M. D., Smith R. C., Martin J. S., 1995, A&A, 302, 90
Stauffer J., Hartmann L., 1986, ApJS, 61, 531
Stone R. P. S., 1977, ApJ, 218, 767
Wade R. A., Horne K., 1988, ApJ, 324, 411
Welsh W. F., Horne K., Gomer R., 1995, MNRAS, 275, 649

APPENDIX A: MEASURED VELOCITIES AND FLUXES

Listed in Tables A1–A5 are the measured velocities and line flux densities (or flux deficits in the case of Na I) for all the lines studied in the paper. The data are tabulated according to the year they were collected, the region of the spectrum (red arm or blue arm), and whether the values were derived from binned spectra or not. The HJDs and phases are for mid-exposure in the unbinned spectra and the average phase in the phase-binned data. With the exception of Na I and Mg II at 4481 Å, the flux values correspond to the average flux density in the line. Thus for a given line, the total flux is some constant factor larger. The value of this factor depends on the number of pixels used in the sum.

Table A1. Measured velocities and line fluxes of the absorption and emission lines in QQ Vul in the red region of the spectrum from the 1991 data.

HJD	Orbital	Na I 8183/8195		Mg II 7877		He II 8236		C I 8335		Ca II 8498/H I 8502	
(+2 448 400)	phase	v (km s^{-1})	f_ν (mJy)	v (km s^{-1})	f_ν(mJy)	v (km s^{-1})	f_ν (mJy)	v (km s^{-1})	f_ν (mJy)	v (km s^{-1})	f_ν (mJy)
46.4897	0.121	163.5 ± 16.6	4.70 ± 1.27	41.9 ± 40.0	0.17 ± 0.02	58.3 ± 15.1	0.33 ± 0.04	…	0.05 ± 0.03	−91.6 ± 24.9	0.13 ± 0.02
46.4997	0.186	194.1 ± 13.6	2.38 ± 11.72	86.5 ± 18.5	0.12 ± 0.02	89.5 ± 6.4	0.50 ± 0.05	…	0.14 ± 0.04	−29.4 ± 5.5	0.37 ± 0.02
46.5121	0.267	251.2 ± 20.2	1.81 ± 0.98	120.4 ± 14.8	0.17 ± 0.02	22.0 ± 23.9	0.53 ± 0.04	129.1 ± 20.5	0.17 ± 0.03	−18.4 ± 4.0	0.35 ± 0.02
46.5219	0.329	225.9 ± 10.3	3.17 ± 0.97	122.9 ± 8.9	0.12 ± 0.02	…	0.41 ± 0.04	111.3 ± 27.0	0.20 ± 0.03	−25.2 ± 2.5	0.47 ± 0.02
46.5331	0.401	205.3 ± 4.3	2.23 ± 0.92	103.5 ± 9.0	0.16 ± 0.02	58.4 ± 11.8	0.39 ± 0.04	55.7 ± 17.0	0.28 ± 0.03	−57.2 ± 2.1	0.54 ± 0.01
46.5424	0.462	…	…	9.2 ± 8.7	0.25 ± 0.02	22.0 ± 13.6	0.47 ± 0.04	75.0 ± 23.2	0.31 ± 0.03	−105.0 ± 2.5	0.57 ± 0.02
46.5516	0.521	…	…	−43.4 ± 12.6	0.13 ± 0.02	−26.4 ± 7.6	0.40 ± 0.05	1.4 ± 14.2	0.35 ± 0.04	−174.6 ± 3.1	0.53 ± 0.02
46.6022	0.849	−189.9 ± 10.1	5.39 ± 0.79	−143.6 ± 40.0	0.03 ± 0.02	…	0.14 ± 0.03	−47.9 ± 68.4	0.05 ± 0.03	−228.7 ± 24.9	0.12 ± 0.02
46.6115	0.909	−147.6 ± 10.4	6.02 ± 0.81	…	0.02 ± 0.02	−29.9 ± 21.9	0.10 ± 0.03	…	0.09 ± 0.03	−216.2 ± 49.9	0.03 ± 0.01
46.6208	0.969	−8.7 ± 22.6	6.24 ± 1.40	…	−0.00 ± 0.01	…	0.05 ± 0.03	…	0.00 ± 0.03	−130.6 ± 27.0	−0.04 ± 0.01
46.6301	0.029	45.0 ± 8.6	5.60 ± 0.77	…	0.04 ± 0.02	…	0.13 ± 0.04	…	0.00 ± 0.03	…	0.05 ± 0.01
46.6412	0.101	130.3 ± 12.5	6.71 ± 1.04	…	0.02 ± 0.02	…	0.28 ± 0.03	…	0.10 ± 0.03	…	0.14 ± 0.01
46.6505	0.161	224.5 ± 21.8	5.89 ± 1.18	…	0.11 ± 0.02	44.6 ± 22.7	0.50 ± 0.05	…	0.06 ± 0.04	−1.6 ± 13.9	0.26 ± 0.02
46.6608	0.228	279.8 ± 15.6	6.24 ± 1.32	82.1 ± 9.5	0.17 ± 0.02	…	0.55 ± 0.03	114.0 ± 22.0	0.18 ± 0.03	−30.4 ± 3.9	0.40 ± 0.02
46.6693	0.283	…	…	…	0.17 ± 0.03	55.7 ± 37.3	0.47 ± 0.05	43.6 ± 21.9	0.21 ± 0.04	−25.6 ± 5.7	0.51 ± 0.02
46.6763	0.328	246.7 ± 34.1	2.45 ± 1.10	…	0.12 ± 0.04	…	0.44 ± 0.06	153.6 ± 22.3	0.16 ± 0.05	−39.8 ± 4.9	0.56 ± 0.03
47.4160	0.116	178.2 ± 7.9	2.99 ± 0.60	…	0.04 ± 0.02	12.8 ± 13.3	0.38 ± 0.03	…	−0.01 ± 0.02	−116.5 ± 24.9	0.13 ± 0.02
47.4257	0.178	238.0 ± 14.2	3.83 ± 0.83	…	0.01 ± 0.02	…	0.24 ± 0.03	…	−0.02 ± 0.02	−14.9 ± 7.3	0.28 ± 0.02
47.4352	0.240	240.3 ± 7.5	4.15 ± 0.67	85.3 ± 13.4	0.14 ± 0.02	98.3 ± 6.4	0.28 ± 0.03	123.7 ± 26.0	0.09 ± 0.03	−36.3 ± 4.4	0.35 ± 0.02
47.4447	0.301	269.2 ± 12.2	2.64 ± 0.73	…	0.12 ± 0.02	80.0 ± 6.0	0.36 ± 0.03	134.0 ± 12.4	0.20 ± 0.02	−22.1 ± 3.7	0.40 ± 0.02
47.4567	0.379	209.9 ± 8.2	1.72 ± 0.63	98.1 ± 11.5	0.07 ± 0.02	54.6 ± 5.3	0.40 ± 0.03	105.5 ± 15.7	0.27 ± 0.03	−52.5 ± 2.9	0.44 ± 0.02
47.4664	0.441	…	…	52.3 ± 14.1	0.09 ± 0.02	40.8 ± 9.4	0.51 ± 0.03	13.2 ± 8.1	0.42 ± 0.02	−97.2 ± 3.3	0.49 ± 0.02
47.4862	0.570	…	…	−56.0 ± 22.5	0.07 ± 0.02	−52.2 ± 6.4	0.40 ± 0.03	−73.3 ± 21.1	0.22 ± 0.02	−230.8 ± 3.1	0.29 ± 0.01
47.4994	0.655	−250.6 ± 14.0	4.03 ± 0.89	−113.1 ± 10.0	0.15 ± 0.02	−62.2 ± 8.1	0.39 ± 0.03	…	0.22 ± 0.02	−276.3 ± 2.5	0.30 ± 0.01
47.5106	0.728	−247.1 ± 13.4	6.19 ± 1.17	−146.4 ± 41.9	0.07 ± 0.02	−36.3 ± 10.1	0.51 ± 0.03	…	0.08 ± 0.03	−263.1 ± 5.2	0.29 ± 0.02
47.5199	0.788	−225.9 ± 16.8	7.42 ± 1.39	…	0.11 ± 0.02	−71.7 ± 7.3	0.32 ± 0.03	…	0.14 ± 0.03	−240.1 ± 9.2	0.15 ± 0.02
47.5293	0.849	−199.8 ± 11.3	7.17 ± 1.10	…	0.09 ± 0.02	−10.2 ± 18.4	0.16 ± 0.03	−43.4 ± 70.7	0.02 ± 0.02	−241.1 ± 37.4	0.10 ± 0.01
47.5386	0.909	−137.7 ± 12.3	4.34 ± 0.73	…	0.05 ± 0.02	−66.1 ± 11.2	0.16 ± 0.02	…	0.02 ± 0.02	…	0.07 ± 0.01
47.5479	0.969	−54.6 ± 11.8	4.37 ± 0.68	…	0.07 ± 0.02	12.5 ± 19.9	0.03 ± 0.02	…	−0.01 ± 0.02	−168.1 ± 11.5	0.02 ± 0.01
47.5647	0.078	109.4 ± 10.9	3.59 ± 0.58	41.9 ± 73.2	0.04 ± 0.02	…	0.12 ± 0.02	…	−0.01 ± 0.02	…	0.07 ± 0.01
47.5740	0.138	205.9 ± 17.2	3.99 ± 0.99	…	0.00 ± 0.02	…	0.28 ± 0.03	…	0.06 ± 0.02	−54.2 ± 37.4	0.17 ± 0.01
47.5833	0.198	218.2 ± 15.4	3.17 ± 0.93	83.7 ± 62.8	0.14 ± 0.02	92.0 ± 5.6	0.39 ± 0.03	…	0.14 ± 0.02	−30.8 ± 4.9	0.31 ± 0.02
47.6146	0.401	186.9 ± 8.5	2.94 ± 0.95	80.9 ± 8.9	0.14 ± 0.02	67.1 ± 5.7	0.42 ± 0.03	61.7 ± 13.5	0.29 ± 0.02	−68.0 ± 2.7	0.46 ± 0.02
47.6448	0.596	−247.8 ± 10.7	3.43 ± 0.93	−52.3 ± 41.9	0.16 ± 0.02	−52.9 ± 7.1	0.53 ± 0.04	−96.2 ± 22.6	0.02 ± 0.03	−253.5 ± 24.9	0.35 ± 0.02
47.6533	0.651	−260.8 ± 16.4	4.10 ± 1.30	−111.1 ± 17.1	0.13 ± 0.02	−77.1 ± 15.3	0.28 ± 0.04	−34.0 ± 53.9	0.18 ± 0.03	−278.8 ± 3.8	0.36 ± 0.02
47.6619	0.707	−261.9 ± 9.8	4.08 ± 0.94	−99.3 ± 14.4	0.09 ± 0.02	…	0.26 ± 0.04	−101.0 ± 46.5	0.06 ± 0.03	−297.5 ± 3.7	0.25 ± 0.02
47.6619	0.707	−261.9 ± 9.8	4.08 ± 0.94	−99.3 ± 14.4	0.09 ± 0.02	…	0.26 ± 0.04	−101.0 ± 46.5	0.06 ± 0.03	−297.5 ± 3.7	0.25 ± 0.02

Table A1 – *continued*

HJD (+2 448 400)	Orbital phase	Data from 1991 Ca II 8542/H I 8545 v (km s^{-1})	Ca II 8542/H I 8545 f_ν(mJy)	H I 8598 v (km s^{-1})	H I 8598 f_ν(mJy)	Ca II 8662/H I 8665 v (km s^{-1})	Ca II 8662/H I 8665 f_ν (mJy)	H I 8750 v (km s^{-1})	H I 8750 f_ν (mJy)
46.4897	0.121	8.4 ± 29.4	0.23 ± 0.01	…	0.29 ± 0.01	…	0.36 ± 0.01	35.2 ± 23.0	0.44 ± 0.01
46.4997	0.186	4.5 ± 3.6	0.43 ± 0.02	89.7 ± 10.2	0.31 ± 0.02	26.4 ± 5.0	0.55 ± 0.02	84.4 ± 7.1	0.61 ± 0.02
46.5121	0.267	7.9 ± 2.1	0.43 ± 0.01	35.5 ± 8.7	0.32 ± 0.01	26.9 ± 2.7	0.51 ± 0.01	38.9 ± 9.6	0.52 ± 0.02
46.5219	0.329	7.9 ± 2.0	0.63 ± 0.02	39.5 ± 13.4	0.35 ± 0.02	27.4 ± 2.7	0.63 ± 0.02	71.7 ± 7.3	0.63 ± 0.02
46.5331	0.401	−21.8 ± 1.4	0.70 ± 0.01	18.0 ± 8.1	0.33 ± 0.01	−4.3 ± 2.1	0.76 ± 0.01	47.9 ± 5.5	0.61 ± 0.01
46.5424	0.462	−74.8 ± 1.8	0.74 ± 0.02	13.5 ± 9.9	0.36 ± 0.02	−47.4 ± 2.2	0.75 ± 0.02	19.2 ± 14.0	0.43 ± 0.02
46.5516	0.521	−133.3 ± 1.9	0.61 ± 0.02	−54.5 ± 7.9	0.21 ± 0.02	−112.3 ± 3.0	0.60 ± 0.02	−11.1 ± 6.8	0.56 ± 0.02
46.6022	0.849	−200.7 ± 12.5	0.17 ± 0.01	…	0.20 ± 0.01	…	0.28 ± 0.01	…	0.38 ± 0.02
46.6115	0.909	…	0.15 ± 0.01	…	0.14 ± 0.01	…	0.18 ± 0.01	−67.5 ± 16.3	0.22 ± 0.01
46.6208	0.969	−111.8 ± 27.2	0.03 ± 0.01	…	0.07 ± 0.01	−163.2 ± 10.9	0.00 ± 0.01	−1.6 ± 29.7	−0.04 ± 0.01
46.6301	0.029	−110.1 ± 27.5	0.01 ± 0.01	…	0.08 ± 0.01	−62.9 ± 17.5	0.13 ± 0.01	−14.0 ± 8.6	0.24 ± 0.01
46.6412	0.101	−11.6 ± 14.7	0.20 ± 0.01	…	0.21 ± 0.01	−3.9 ± 18.0	0.24 ± 0.01	…	0.38 ± 0.01
46.6505	0.161	−2.0 ± 3.7	0.38 ± 0.01	…	0.35 ± 0.01	13.7 ± 3.5	0.46 ± 0.01	76.3 ± 7.4	0.48 ± 0.02
46.6608	0.228	−2.6 ± 2.0	0.52 ± 0.02	66.2 ± 7.2	0.31 ± 0.01	24.3 ± 2.3	0.63 ± 0.01	96.6 ± 6.0	0.67 ± 0.02
46.6693	0.283	4.7 ± 2.4	0.59 ± 0.02	54.5 ± 10.6	0.40 ± 0.02	27.1 ± 2.9	0.59 ± 0.02	61.6 ± 10.1	0.60 ± 0.02
46.6763	0.328	12.1 ± 3.6	0.60 ± 0.03	34.3 ± 11.3	0.46 ± 0.03	1.8 ± 3.8	0.80 ± 0.03	71.0 ± 16.9	0.65 ± 0.03
47.4160	0.116	−63.7 ± 24.9	0.17 ± 0.01	111.5 ± 51.6	0.21 ± 0.01	…	0.33 ± 0.01	81.3 ± 13.9	0.26 ± 0.02
47.4257	0.178	2.2 ± 3.7	0.32 ± 0.01	137.9 ± 14.0	0.26 ± 0.01	25.0 ± 4.9	0.40 ± 0.01	122.7 ± 20.6	0.49 ± 0.01
47.4352	0.240	3.4 ± 2.6	0.36 ± 0.02	103.6 ± 18.4	0.24 ± 0.02	24.6 ± 3.7	0.46 ± 0.02	79.6 ± 12.8	0.38 ± 0.02
47.4447	0.301	20.4 ± 2.3	0.56 ± 0.01	58.5 ± 8.0	0.29 ± 0.01	32.7 ± 2.6	0.58 ± 0.01	127.3 ± 11.4	0.52 ± 0.01
47.4567	0.379	−8.4 ± 2.0	0.61 ± 0.02	44.7 ± 17.4	0.29 ± 0.02	6.7 ± 2.9	0.69 ± 0.02	60.3 ± 10.7	0.60 ± 0.02
47.4664	0.441	−58.4 ± 1.7	0.65 ± 0.02	34.5 ± 10.8	0.34 ± 0.02	−39.6 ± 2.7	0.74 ± 0.01	38.7 ± 6.6	0.55 ± 0.02
47.4862	0.570	−176.2 ± 2.2	0.49 ± 0.01	−42.1 ± 14.0	0.24 ± 0.01	−152.8 ± 2.0	0.65 ± 0.01	−80.4 ± 14.1	0.48 ± 0.01
47.4994	0.655	−231.3 ± 1.9	0.39 ± 0.01	−130.8 ± 12.7	0.22 ± 0.01	−210.8 ± 3.1	0.48 ± 0.01	−114.4 ± 12.4	0.41 ± 0.02
47.5106	0.728	−215.9 ± 3.2	0.39 ± 0.02	−105.2 ± 11.2	0.26 ± 0.01	−207.1 ± 5.2	0.48 ± 0.02	…	0.47 ± 0.02
47.5199	0.788	−238.1 ± 24.9	0.24 ± 0.02	…	0.24 ± 0.01	…	0.38 ± 0.01	…	0.36 ± 0.01
47.5293	0.849	−188.3 ± 24.9	0.15 ± 0.01	…	0.18 ± 0.01	…	0.24 ± 0.01	…	0.29 ± 0.02
47.5386	0.909	…	0.11 ± 0.01	…	0.14 ± 0.01	…	0.13 ± 0.01	…	0.16 ± 0.01
47.5479	0.969	…	0.00 ± 0.01	…	0.04 ± 0.01	…	−0.02 ± 0.01	…	0.08 ± 0.01
47.5647	0.078	…	0.07 ± 0.01	…	0.09 ± 0.01	…	0.18 ± 0.01	…	0.24 ± 0.01
47.5740	0.138	−18.0 ± 9.0	0.23 ± 0.01	119.6 ± 15.1	0.22 ± 0.01	25.3 ± 4.3	0.31 ± 0.01	…	0.37 ± 0.02
47.5833	0.198	4.3 ± 3.0	0.33 ± 0.01	81.3 ± 8.2	0.37 ± 0.02	21.2 ± 3.5	0.55 ± 0.02	107.3 ± 18.0	0.66 ± 0.02
47.6146	0.401	−23.0 ± 2.0	0.65 ± 0.01	25.3 ± 6.4	0.34 ± 0.01	−12.9 ± 2.2	0.64 ± 0.01	41.2 ± 5.7	0.56 ± 0.01
47.6448	0.596	−213.7 ± 2.1	0.49 ± 0.02	−105.5 ± 9.9	0.36 ± 0.02	−195.8 ± 2.6	0.62 ± 0.01	−76.2 ± 8.8	0.57 ± 0.02
47.6533	0.651	−241.6 ± 2.1	0.47 ± 0.02	−189.6 ± 12.7	0.31 ± 0.02	−236.2 ± 3.7	0.55 ± 0.02	−108.0 ± 11.5	0.45 ± 0.02
47.6619	0.707	−242.8 ± 2.2	0.35 ± 0.01	−140.1 ± 11.0	0.32 ± 0.01	−221.5 ± 6.1	0.45 ± 0.01	−133.1 ± 7.0	0.52 ± 0.02

Table A2. The velocities and line fluxes of Mg II at 7896 Å in emission derived from the 1991 phase binned spectra.

Orbital phase	Mg II 7896 v (km s^{-1})	f_ν(mJy)
0.029	−21.4 ± 53.7	0.12 ± 0.01
0.078	16.8 ± 16.2	0.06 ± 0.01
0.119	19.7 ± 13.2	0.15 ± 0.01
0.181	63.6 ± 3.7	0.19 ± 0.01
0.234	76.3 ± 6.3	0.17 ± 0.01
0.273	70.0 ± 9.2	0.17 ± 0.01
0.318	89.4 ± 7.9	0.22 ± 0.01
0.379	80.8 ± 4.1	0.19 ± 0.01
0.415	60.3 ± 3.8	0.17 ± 0.01
0.462	25.3 ± 5.3	0.15 ± 0.01
0.521	−30.2 ± 3.8	0.21 ± 0.02
0.582	−63.4 ± 9.0	0.17 ± 0.01
0.653	−139.0 ± 6.7	0.19 ± 0.01
0.718	−127.4 ± 20.4	0.11 ± 0.01
0.788	−91.2 ± 62.7	0.10 ± 0.01
0.969	−44.0 ± 14.6	0.09 ± 0.01

Table A3. The velocities and total line fluxes of Mg II at 4481 Å in emission from the 1991 and 1993 spectra.

Data from 1991

HJD (+2 448 400)	Orbital phase	Mg II 4481 v (km s^{-1})	f_ν(mJy)
46.5120	0.265	84.2 ± 6.3	2.71 ± 0.48
46.5218	0.328	111.6 ± 4.0	2.41 ± 0.35
46.5330	0.401	94.2 ± 2.8	3.16 ± 0.35
46.5423	0.461	52.4 ± 3.0	3.63 ± 0.36
46.5515	0.521	−13.1 ± 3.5	3.87 ± 0.40
46.5608	0.581	−88.2 ± 3.8	3.32 ± 0.38
46.6607	1.227	105.9 ± 4.5	2.69 ± 0.40
46.6692	1.283	92.9 ± 8.9	2.75 ± 0.53
47.4351	6.239	80.4 ± 5.1	1.94 ± 0.28
47.4446	6.301	83.1 ± 5.9	2.69 ± 0.48
47.4566	6.378	85.4 ± 3.6	2.84 ± 0.40
47.4663	6.441	51.2 ± 3.1	3.34 ± 0.37
47.4768	6.509	−9.1 ± 3.7	3.30 ± 0.38
47.4861	6.569	−81.7 ± 5.2	2.19 ± 0.35
47.5198	6.787	−122.5 ± 19.7	0.78 ± 0.33
47.5832	7.197	90.0 ± 5.5	3.20 ± 0.47
47.6145	7.400	71.9 ± 5.3	2.55 ± 0.38
47.6447	7.595	−89.7 ± 5.6	2.56 ± 0.45
47.6532	7.651	−140.0 ± 12.4	1.10 ± 0.34
47.6618	7.706	−134.2 ± 8.4	4.74 ± 0.87

Data from 1993

HJD (+2 449 200)	Orbital phase	Mg II 4481 v (km s^{-1})	f_ν(mJy)
23.4132	0.097	21.4 ± 21.4	0.23 ± 0.26
23.4208	0.147	96.9 ± 5.8	4.30 ± 0.35
23.4246	0.171	76.8 ± 4.8	4.13 ± 0.33
23.4285	0.196	80.9 ± 3.3	4.02 ± 0.37
23.4372	0.252	66.6 ± 5.8	3.61 ± 0.42
23.4410	0.277	89.6 ± 5.7	3.31 ± 0.52
23.4448	0.302	109.8 ± 4.6	2.85 ± 0.36
23.4487	0.327	105.2 ± 3.9	3.04 ± 0.35
23.4657	0.437	54.6 ± 3.8	2.98 ± 0.35
24.4448	0.773	−121.3 ± 23.4	5.14 ± 1.42
25.4399	0.213	88.7 ± 4.8	3.88 ± 0.39
25.4437	0.238	69.2 ± 7.1	3.41 ± 0.47
25.4475	0.263	101.1 ± 5.9	3.05 ± 0.49
25.4513	0.287	106.7 ± 8.6	3.08 ± 0.57
25.4551	0.312	114.3 ± 6.9	3.50 ± 0.48
25.4590	0.337	108.6 ± 5.4	3.62 ± 0.46
25.4666	0.386	83.5 ± 4.9	3.28 ± 0.39
25.4704	0.411	81.1 ± 4.8	3.97 ± 0.49
25.4743	0.436	52.7 ± 4.3	4.51 ± 0.51
25.4850	0.505	3.6 ± 5.8	3.58 ± 0.42
25.4888	0.530	−10.3 ± 4.8	3.33 ± 0.49
25.4926	0.555	−45.3 ± 6.8	3.22 ± 0.44
25.4964	0.579	−55.2 ± 5.3	3.39 ± 0.40
25.5003	0.604	−79.5 ± 6.7	3.64 ± 0.47
25.5041	0.629	−101.7 ± 5.8	6.42 ± 0.79
25.5079	0.654	−104.0 ± 8.1	3.44 ± 0.62
25.5117	0.678	−91.5 ± 8.7	1.76 ± 0.38

Table A4. The velocities and flux deficits of the Na I absorption doublet from the 1993 data.

HJD (+2 449 200)	Orbital phase	Na I 8183/8195 v (km s^{-1})	f_ν (mJy)
23.4063	0.053	114.1 ± 23.0	5.08 ± 0.83
23.4131	0.097	74.1 ± 20.2	5.08 ± 0.83
23.4173	0.124	95.8 ± 5.2	5.63 ± 1.17
23.4213	0.150	137.0 ± 9.2	5.63 ± 1.17
23.4254	0.176	189.4 ± 24.9	4.97 ± 1.39
23.4294	0.202	173.7 ± 15.9	3.78 ± 1.10
23.4371	0.252	287.1 ± 17.4	3.71 ± 1.03
23.4413	0.279	301.6 ± 7.9	3.71 ± 1.03
23.4453	0.305	205.8 ± 29.8	3.99 ± 1.23
23.4493	0.331	207.7 ± 10.9	3.99 ± 1.23
23.4534	0.357	247.4 ± 12.3	2.31 ± 0.81
23.4574	0.384	218.2 ± 20.8	2.31 ± 0.81
23.4657	0.437	138.2 ± 9.4	0.97 ± 0.76
24.4448	0.773	−198.1 ± 10.0	9.77 ± 1.63
24.4488	0.800	−166.1 ± 11.3	9.77 ± 1.63
24.4529	0.826	−125.5 ± 23.8	7.99 ± 1.63
24.4610	0.878	−136.0 ± 7.5	8.75 ± 1.36
24.4650	0.904	−130.1 ± 6.1	4.36 ± 0.82
24.4691	0.931	−126.1 ± 32.9	4.36 ± 0.82
24.4731	0.957	−121.5 ± 10.5	5.92 ± 0.73
24.4772	0.983	−20.2 ± 6.4	5.92 ± 0.73
24.4812	0.009	−14.9 ± 12.1	3.87 ± 0.70
24.4916	0.077	−19.1 ± 7.2	5.08 ± 0.83
25.3955	0.926	−72.6 ± 37.4	4.36 ± 0.82
25.3996	0.953	−91.6 ± 9.9	5.92 ± 0.73
25.4036	0.979	−40.4 ± 6.4	5.92 ± 0.73
25.4077	0.005	−47.0 ± 9.1	3.87 ± 0.70
25.4117	0.031	−26.3 ± 16.5	3.87 ± 0.70
25.4157	0.057	37.3 ± 5.8	5.08 ± 0.83
25.4198	0.083	80.5 ± 90.9	5.08 ± 0.83
25.4238	0.109	66.6 ± 9.8	5.63 ± 1.17
25.4278	0.135	85.5 ± 7.5	5.63 ± 1.17
25.4318	0.161	177.6 ± 7.4	4.97 ± 1.39
25.4399	0.213	209.5 ± 6.5	3.78 ± 1.10
25.4439	0.239	200.1 ± 8.3	3.78 ± 1.10
25.4480	0.266	240.6 ± 5.1	3.71 ± 1.03
25.4520	0.292	257.8 ± 8.9	3.71 ± 1.03
25.4560	0.318	236.6 ± 15.6	3.99 ± 1.23
25.4601	0.344	240.8 ± 6.9	3.99 ± 1.23
25.4641	0.370	214.9 ± 6.1	2.31 ± 0.81
25.4681	0.396	170.4 ± 9.1	2.31 ± 0.81
25.4722	0.422	98.1 ± 17.6	0.97 ± 0.76
25.5012	0.610	−212.7 ± 11.0	6.36 ± 1.45
25.5052	0.636	−230.0 ± 5.9	6.36 ± 1.45
25.5092	0.662	−203.8 ± 46.8	6.07 ± 1.33
25.5133	0.688	−214.2 ± 7.6	6.07 ± 1.33
25.5173	0.714	−229.7 ± 18.5	6.10 ± 1.34
25.5207	0.737	−193.1 ± 28.0	6.10 ± 1.34
25.5293	0.792	−200.8 ± 33.3	9.77 ± 1.63
25.5334	0.819	−198.5 ± 19.9	7.99 ± 1.63
25.5375	0.845	−144.4 ± 24.5	7.99 ± 1.63
25.5415	0.871	−116.1 ± 10.4	8.75 ± 1.36
25.5455	0.897	−148.1 ± 100.7	8.75 ± 1.36
25.5542	0.953	−17.5 ± 21.0	5.92 ± 0.73

Table A5. The velocities and emission line fluxes of He II at 8236 Å and C I at 8335 Å, derived from the 1993 phase-binned data.

Orbital phase	He II 8236 v (km s^{-1})	f_ν (mJy)	C I 8335 v (km s^{-1})	f_ν (mJy)
0.015	…	0.08 ± 0.04	−38.8 ± 28.3	0.02 ± 0.04
0.055	39.4 ± 35.7	0.20 ± 0.04	−3.8 ± 21.2	−0.01 ± 0.03
0.085	…	0.14 ± 0.04	0.2 ± 11.6	0.03 ± 0.04
0.116	−13.9 ± 18.9	0.49 ± 0.05	45.9 ± 14.4	0.06 ± 0.04
0.149	65.0 ± 7.2	0.50 ± 0.04	54.4 ± 25.7	0.03 ± 0.03
0.176	67.0 ± 6.7	0.89 ± 0.07	44.9 ± 24.7	0.19 ± 0.04
0.208	48.7 ± 10.3	0.71 ± 0.05	…	0.05 ± 0.04
0.252	23.0 ± 8.8	0.68 ± 0.04	44.1 ± 10.8	0.30 ± 0.03
0.285	54.0 ± 12.6	0.60 ± 0.05	24.6 ± 27.2	0.19 ± 0.04
0.318	66.0 ± 11.1	0.66 ± 0.03	51.4 ± 8.3	0.35 ± 0.02
0.351	68.4 ± 7.3	0.68 ± 0.04	70.2 ± 14.2	0.44 ± 0.04
0.383	−16.0 ± 17.7	0.59 ± 0.03	66.9 ± 8.8	0.37 ± 0.03
0.422	59.5 ± 14.5	0.76 ± 0.06	18.9 ± 27.6	0.30 ± 0.05
0.443	2.4 ± 6.8	0.72 ± 0.04	35.5 ± 6.9	0.37 ± 0.03
0.518	−11.4 ± 5.9	0.57 ± 0.04	−56.5 ± 10.4	0.36 ± 0.04
0.558	−32.1 ± 6.8	0.66 ± 0.07	−6.0 ± 36.9	0.32 ± 0.08
0.584	−43.1 ± 11.9	0.56 ± 0.07	−93.0 ± 30.2	0.07 ± 0.07
0.610	−35.8 ± 6.7	0.59 ± 0.05	−56.8 ± 10.3	0.46 ± 0.06
0.649	−32.8 ± 9.4	0.86 ± 0.07	−91.6 ± 6.6	0.25 ± 0.04
0.688	−51.8 ± 6.2	0.93 ± 0.08	−40.3 ± 26.0	0.11 ± 0.06
0.714	−26.8 ± 26.8	0.82 ± 0.12	−39.4 ± 40.4	0.11 ± 0.08
0.737	−40.6 ± 10.8	0.57 ± 0.12	−113.5 ± 25.3	0.20 ± 0.09
0.788	−2.0 ± 17.5	0.43 ± 0.05	−25.0 ± 15.1	0.15 ± 0.05
0.822	−49.2 ± 23.4	0.24 ± 0.07	−13.4 ± 25.8	0.19 ± 0.06
0.845	…	0.24 ± 0.07	−48.4 ± 11.5	0.19 ± 0.04
0.882	…	0.18 ± 0.04	2.6 ± 12.4	0.13 ± 0.03
0.920	…	−0.02 ± 0.04	−9.2 ± 19.0	0.15 ± 0.04
0.954	6.9 ± 16.0	0.03 ± 0.04	25.4 ± 11.3	0.14 ± 0.04
0.981	13.8 ± 13.9	0.19 ± 0.04	…	0.09 ± 0.04

This paper has been typeset from a TEX/LATEX file prepared by the author.